Analytical and numerical evaluation of quarter-elliptic-braced steel moment frames (QEB-MFs)

Nader Fanaie [*], Alireza Shirpour

Department of Civil Engineering, K. N. Toosi University of Technology, Tehran, Iran

A R T I C L E   I N F O

A B S T R A C T

Concentrically braced frames (CBFs) have an excellent performance to the lateral seismic forces at the time of the mild earthquakes, but they are weak under severe seismic loads due to the occurrence of buckling of the bracing members and the lack of proper ductility in terms of energy absorption and do not behave properly. This article introduces the new quarter-elliptic brace. Adding this brace to the moment frame improves the stiffness of this system and impedes the excess structural deformation in this system. In the present study, a precise analytical formulation is presented using the concept of strain energy and Castigliano's theorem in order to calculate the elastic lateral stiffness of a two-dimensional single-span and single-story steel moment frame equipped with quarter-elliptic brace. In this relation, all effective factors, including axial and shear forces as well as bending moment, were considered for all frame members. The proposed formulation was controlled by the results of various examples in OpenSees software. The error percentage between the results obtained from the newly developed formulation and numerical analysis of finite elements is very insignificant so that it can be ignored. Also, the seismic performance of this system was investigated according to the FEMA P695 methodology for near-field and far-field ground motion records compared with the intermediate moment frame. The results showed that using a quarter-elliptic brace in the intermediate moment frame improves the seismic performance of this system.

1. Introduction

Steel CBFs, due to considerable lateral stiffness, high lateral strength, and ease of implementation, are among the most widely used structural systems in constructing steel structures. One of the problems of CBFs is the occurrence of buckling when applying compressive load, which causes instability before reaching the yield strength. In other words, the behavior of braces, in tension and compression, is asymmetrical, and as a result, the hysteresis curves of these types of bracing frames become irregular. In addition, CBFs have limited ductility and energy dissipation and have high elastic stiffness. Thus, ordinary braces have limited ductility capacity and asymmetric force–displacement loops [1–7]. In recent decades, researchers have conducted extensive research on this structural system and have developed various methods to increase the ductility of common CBFs. The majority of methods used for the ductility of bracing steel structures included the use of buckling restrained brace (BRB) instead of conventional braces and the use of structural fuses locally and in certain parts of the brace throughout the length of the brace or bracing connections [8–15].

Off-center bracing system (OBS) is one of the systems developed in order to improve the concentrically braced structures. In this structural system, the bracing element is not direct, and therefore, its primary geometry changes when a lateral load is imposed into this system. So, the force–displacement curve of these systems is geometrically nonlinear, and the degree of nonlinearity of this system is mainly dependent on the off-centrality and relative stiffness of the bracing elements [16]. In their study on these systems, Moghaddam and Estekanchi found that the force–displacement curve in these systems follows a nonlinear hardening pattern with two yield points. Then, using this model, the structures of single-story and multi-story were subjected to seismic loads. The results of these analyses indicated that this structural system has a behavioral like that of base isolation systems and has a good strength to lateral loads [17]. Trombetti et al. (2009), in a framework design based on stiffness, strength, and ductility, introduced a new hysteretic member called crescent shaped brace (CSB) [18]. They showed the capability of crescent shaped members using them in a 5-

---

story steel frame designed based on the concept of isolation considering the first soft-story [19]. Their results showed that the crescent shaped members placed on the first story, due to their specific geometry with symmetric cyclic behavior and hardening in high escapes (due to geometric nonlinearity), can prevent total instability caused by the second-order effects. In 2015, Palermo et al. conducted comprehensive laboratory studies on crescent shaped braces (Fig. 1). The results showed that the initial lateral stiffness and initial yield strength are independent in these braces, and these braces have considerable ductility capacity and final hardening in order to prevent damage caused by the second-order effects. These braces, due to their geometric structure, in addition to further energy dissipation, also allow to adjust the stiffness to the desired amount [20,21]. In Fig. 1, the knee point distance has been denoted by d. Seismic performance factors in the crescent-shaped bracing system depend on the value of d. Because this distance is variable, it is impossible to present constant seismic performance factors for this system.

In 2016, Jouneghani et al. introduced the new elliptic brace, and in 2018, Boostani et al. introduced the circular brace (OGrid) (Fig. 2a). In addition to improving structural behavior and higher energy dissipation in the structural system, these two braces do not suffer from the lack of architectural space in order to create the opening. One of the worst disadvantages of these two braces is the connection of the bracing members to the columns because a failure to properly connect them and the insertion of excess shear force from the braces to the column might lead to the emergence of plastic hinges in the middle of the column [22–26]. In 2019, Shamivand and Akbari introduced a new ring-shaped brace called Shami lateral bracing system (SLB) (Fig. 2b) and used quasi columns in order to fix the problem of connecting the brace to the main columns [27].

In 1972, Davis et al. obtained the stiffness matrix of a finite element using force–displacement equations based on differential equations of an infinitesimal element in static equilibrium, and the effect of shear deformations is also considered [28,29]. In 1981, Yoo and Fehrenbach presented a curved element of finite elements for the free vibration of a horizontally curved beam, in which the effect of shear deformations was ignored [30]. In 2006, Yoon et al. investigated the out-of-plane dynamic behavior of thin-wall curved beams as a follow-up study to the research developed by Yang and Kuo. They obtained the governing equations on the behavior of thin-wall curved beams with seven degrees of freedom per node, in which the warping effect has also been taken into account [31,32]. In 2009, Kim et al. presented a very thin curved beam element in which the transverse shear effect, transverse rotary inertia force, and torsional rotary inertia force were considered. The stiffness matrix was obtained using strain energy and natural shape functions by integration of differential equations obtained from static equilibrium [33]. In 2016, a new curved beam element with two nodes and six degrees of freedom in order to model arches with parabolic geometry was proposed by Rezaiee and Rajabzadeh, and using the stiffness-based finite elements

method, an explicit stiffness matrix was introduced for the element. They stated that the use of the proposed explicit form of the stiffness matrix of the curved beam could significantly accelerate the process of analysis [34]. In 2018, Marotta and Salvini presented a closed solution to the stiffness matrix of the curved beam using Castigliano's second theorem and considering the bending and axial effects. This analytical solution for a curved beam was carried out through cubic function of radius of curvature. They concluded that this method is also suitable for nonlinear analysis with high displacements [35].

In this paper, a new quarter-elliptic brace is introduced, and the elastic stiffness of the steel moment frame equipped with this brace is accurately calculated. By adding this brace to the moment frame, the stiffness in this system is improved, and excessive structural deformation is prevented in this system. In this research, first, a precise and practical formulation is presented using a new and innovative method in order to calculate the elastic stiffness of the two-dimensional single-span and single-story quarter-elliptic-braced steel moment frame (QEB-MF) under lateral force. In this relation, all effective factors, including axial and shear forces as well as bending moment, were considered for all frame members. This relation was evaluated with different examples in OpenSees finite element software. Then, the seismic performance of this system was investigated according to the FEMA P695 methodology for near-field and far-field ground motion records compared with the intermediate moment frame (IMF). The results showed that using a quarter-elliptic brace in the intermediate moment frame improves the seismic performance of this system.

2. Presenting a new method for calculating the elastic stiffness of QEB-MF systems

In this section of the study, the elastic lateral stiffness of a two-dimensional single-span and single-story QEB-MF system that is under the lateral load of P according to Fig. 3a, using the new method based on the concept of strain energy and Castigliano's theorem, and considering the axial, shear, and bending deformations is determined [36]. According to Fig. 3b, the length of the beam (L_b) is considered to be semi-major axis of the ellipse (a), and the length of the column (L_c) is equal to the semi-minor axis of the ellipse (b). Also, the properties of beam, column, and quarter-elliptic bracing member cross-sections are considered as parametric. The geometric specifications of the frame are expressed according to Fig. 3b in Eq. (1):

$$\tan\theta = \frac{b}{a} = \frac{L_c}{L_b} = e \ ,$$
$$\sin\theta = \frac{b}{\sqrt{a^2+b^2}} = \frac{e}{\sqrt{1+e^2}} \ ,$$
$$\cos\theta = \frac{a}{\sqrt{a^2+b^2}} = \frac{1}{\sqrt{1+e^2}}$$

(1)

In this equation, θ is a parameter for the expression of the frame diameter angle.

Internal efforts of the studied frame under lateral force of P and considering F_{AC} and F_{CA} as forces of the two sides of quarter-elliptic brace cross-section were shown in Fig. 4.

Using compatibility equations for nodes A, B, C, and D, internal efforts for frame members were calculated according to Fig. 5:

For node A (Fig. 5a):

$$M_{AB} = M_{AD} = M_A$$

(2)

For node B (Fig. 5b):

$$M_{BC} = M_{BA} = M_B$$

(3)

$$\sum F_x = 0 \rightarrow P + N_{BC} + V_{BA} = 0$$
$$\rightarrow N_{BC} = -(P + V_{BA})$$

(4)

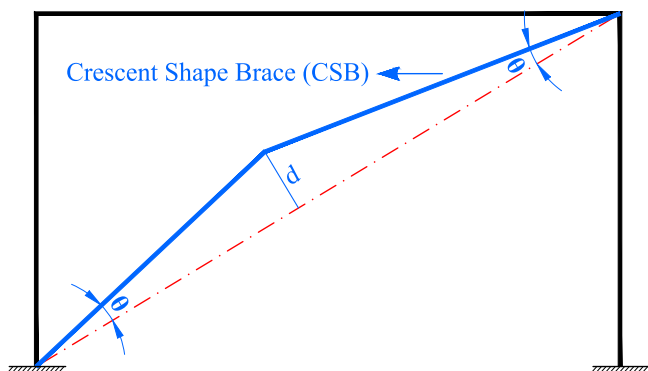$$\sum F_y = 0 \rightarrow N_{BA} = V_{BC}$$

(5)

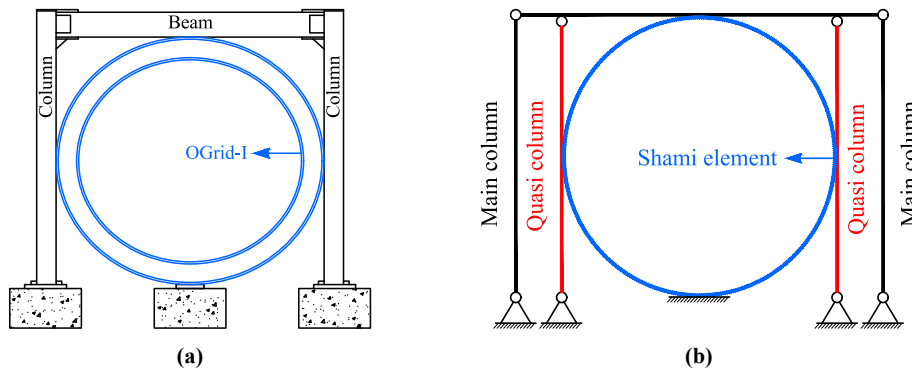**Fig. 1.** A bilinear CSB inserted into a frame as diagonal brace [20].

Fig. 2. (a) Shami lateral bracing system (SLB), (b) OGrid-I bracing system [25,27].
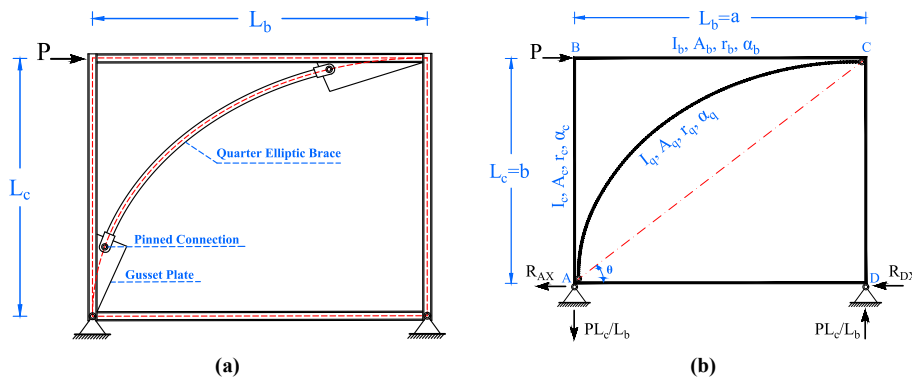

Fig. 3. (a) The desired steel moment frame with directly welded rigid connections equipped with quarter-elliptic brace, (b) Side view of QEB-MF systems.
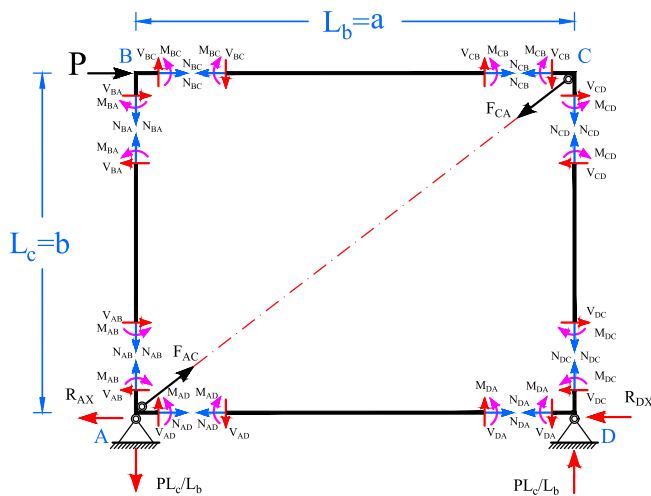

Fig. 4. The internal efforts of the QEB-MFs.

Fig. 5. Analysis of joints in the QEB-MFs; (a) joint *A*, (b) joint *B*, (c) joint *C*, (d) joint *D*.

For node *C* (Fig. 5c):

$$M_{CB} = M_{CD} = M_C \tag{6}$$

$$\sum F_x = 0 \rightarrow V_{CD} - N_{CB} - F_{CA}\cos\theta = 0$$
$$\rightarrow F_{CA} = \frac{V_{CD} - N_{CB}}{\cos\theta} \tag{7}$$

For node *D* (Fig. 5d):

$$M_{DC} = M_{DA} = M_D \tag{8}$$

$$\sum F_y = 0 \rightarrow N_{DC} = V_{DA} - \frac{PL_c}{L_b} \tag{9}$$

The internal efforts of columns *AB* and *DC* and beams *AD* and *BC* were shown in Fig. 6. Using static equilibrium equations and calculation of moment value in the two end nodes of columns and beams, shear and axial forces are calculated on both sides of the members:

For column *AB* (Fig. 6a):

$$N_{AB} = N_{BA} \tag{10}$$

$$\sum M_A = 0 \rightarrow V_{BA} = -\frac{M_{AB} + M_{BA}}{L_c} \tag{11}$$

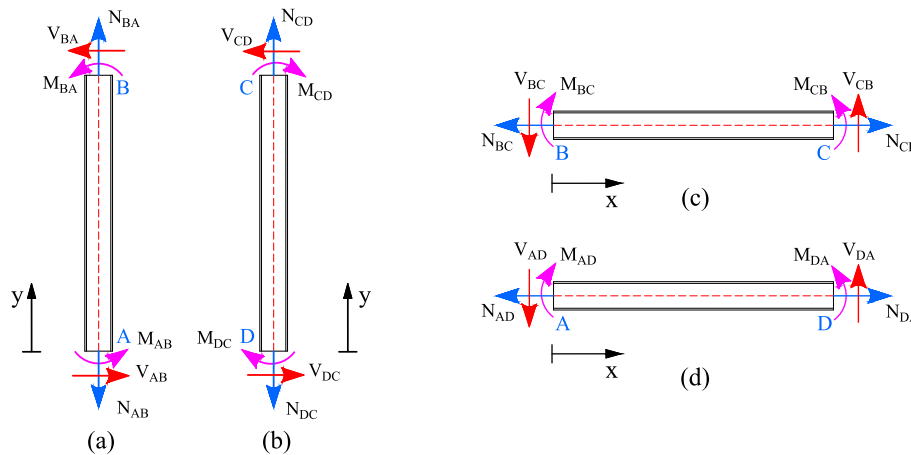**Fig. 6.** The internal efforts; (a) column *AB*, (b) column *DC*, (c) beam *BC*, (d) beam *AD*.

$$\sum M_B = 0 \rightarrow V_{AB} = -\frac{M_{AB} + M_{BA}}{L_c} \tag{12}$$

By inserting Eqs. (2) and (3) in Eqs. (11) and (12), we can conclude that:

$$V_{AB} = V_{BA} = -\frac{M_A + M_B}{L_c} \tag{13}$$

For column *DC* (Fig. 6b):

$$N_{CD} = N_{DC} \tag{14}$$

$$\sum M_C = 0 \rightarrow V_{DC} = \frac{M_{DC} + M_{CD}}{L_c} \tag{15}$$

$$\sum M_D = 0 \rightarrow V_{CD} = \frac{M_{DC} + M_{CD}}{L_c} \tag{16}$$

By inserting Eqs. (6) and (8) in Eqs. (15) and (16), we can conclude that:

$$V_{CD} = V_{DC} = \frac{M_D + M_C}{L_c} \tag{17}$$

For beam *BC* (Fig. 6c):

$$N_{BC} = N_{CB} \tag{18}$$

$$\sum M_B = 0 \rightarrow V_{CB} = \frac{M_{BC} - M_{CB}}{L_b} \tag{19}$$

$$\sum M_C = 0 \rightarrow V_{BC} = \frac{M_{BC} - M_{CB}}{L_b} \tag{20}$$

By inserting Eqs. (3) and (6) in Eqs. (19) and (20), we can conclude that:

$$V_{CB} = V_{BC} = \frac{M_B - M_C}{L_b} \tag{21}$$

For beam *AD* (Fig. 6d):

$$\delta_{AD} = \delta_{DA} = 0 \rightarrow N_{AD} = N_{DA} = 0 \tag{22}$$

$$\sum M_A = 0 \rightarrow V_{DA} = \frac{M_{AD} - M_{DA}}{L_b} \tag{23}$$

$$\sum M_D = 0 \rightarrow V_{AD} = \frac{M_{AD} - M_{DA}}{L_b} \tag{24}$$

Because of the existence of support on both sides of the beam *AD* and the absence of axial force throughout the beam, the axial deformation on the two sides of this beam is equal to zero; therefore, considering $\delta = NL/EA$, the axial force at the two sides of this member is also equal to zero. By

inserting Eqs. (2) and (8) in Eqs. (19) and (20), we can conclude that:

$$V_{DA} = V_{AD} = \frac{M_A - M_D}{L_b} \tag{25}$$

With the placement of Eqs. (13) and (18) in Eq. (4), a new equation has been obtained, so that by inserting this equation and Eq. (17) in Eq. (7), internal efforts of the quarter-elliptic bracing member are calculated as follows:

$$
\begin{aligned}
F_{AC} = F_{CA} &= \frac{P + V_{CD} + V_{BA}}{\cos\theta} \\
&= \frac{P + \dfrac{(M_D + M_C)}{L_c} - \dfrac{(M_A + M_B)}{L_c}}{\cos\theta} \\
&= \frac{PL_c - M_A - M_B + M_D + M_C}{L_c \cos\theta}
\end{aligned}
\tag{26}
$$

The shear modulus of steel (*G*) is obtained based on Young's modulus (*E*) and Poisson's ratio (ν) in Eq. (27):

$$G = \frac{E}{2(1+\nu)}, \nu = 0.3 \rightarrow G = \frac{E}{2(1+0.3)} = \frac{E}{2.6} \tag{27}$$

The total area and effective shear area was obtained for column cross-section in Eq. (28), for beam cross-section in Eq. (29), and for quarter-elliptic brace cross-section in Eq. (30) and according to Fig. 2b:

$$A_c' = \frac{A_c}{\alpha_c}, \quad A_c = \frac{I_c}{r_c^2} \tag{28}$$

$$A_b' = \frac{A_b}{\alpha_b}, \quad A_b = \frac{I_b}{r_b^2} \tag{29}$$

$$A_q' = \frac{A_q}{\alpha_q}, \quad A_q = \frac{I_q}{r_q^2} \tag{30}$$

In these equations, *A* is the cross-sectional area, A' is the effective shear area of the cross-section, α is the shear shape coefficient of the cross-section, and *I* and *r* are the moment of inertia and radius of gyration of the cross-section about the bending axis (strong axis), respectively.

2.1. Calculating strain energy of the columns

Strain energy for columns is calculated under the effect of internal bending moment, internal axial force, and internal shear force. To calculate strain energy in the columns, first, we obtained the equation of internal force changes in columns *AB* and *DC* according to Fig. 6a and b, and then, using the general energy equation, we obtained the amount of strain energy stored in the columns. The internal moment values of the columns were obtained by Eqs. (31) and (32):

$$M_{AB}(y) = M_{AB} + V_{AB}y, \quad 0 \le y \le L_c \tag{31}$$

$$M_{DC}(y) = M_{DC} - V_{DC}y, \quad 0 \le y \le L_c \tag{32}$$

Strain energy values due to bending, axial, and shear deformations for columns were calculated by Eqs. (33) and (34). In these equations, E is Young's modulus and G is shear modulus of steel that is obtained in Eq. (27). Also, A_c is the area of column cross-section, and A_c' is the effective shear area of the column cross-section obtained in Eq. (28).

$$
\begin{aligned}
U_{AB} &= \frac{1}{2EI_c} \int_0^{L_c} M_{AB}^2(y)dy + \frac{V_{AB}^2 L_c}{2GA_c'} + \frac{N_{AB}^2 L_c}{2EA_c} \\
&= \frac{1}{2EI_c} \int_0^{L_c} (M_{AB} + V_{AB}y)^2 dy + 2.6\alpha_c \frac{V_{AB}^2 L_c}{2EA_c} + \frac{N_{AB}^2 L_c}{2EA_c} \\
&= \frac{M_{AB}^2 L_c}{2EI_c} + \frac{M_{AB}V_{AB}L_c^2}{2EI_c} + \frac{V_{AB}^2 L_c^3}{6EI_c} + \frac{(2.6\alpha_c V_{AB}^2 + N_{AB}^2)L_c r_c^2}{2EI_c}
\end{aligned} \tag{33}
$$

$$
\begin{aligned}
U_{DC} &= \frac{1}{2EI_c} \int_0^{L_c} M_{DC}^2(y)dy + \frac{V_{DC}^2 L_c}{2GA_c'} + \frac{N_{DC}^2 L_c}{2EA_c} \\
&= \frac{1}{2EI_c} \int_0^{L_c} (M_{DC} - V_{DC}y)^2 dy + 2.6\alpha_c \frac{V_{DC}^2 L_c}{2EA_c} + \frac{N_{DC}^2 L_c}{2EA_c} \\
&= \frac{M_{DC}^2 L_c}{2EI_c} - \frac{M_{DC}V_{DC}L_c^2}{2EI_c} + \frac{V_{DC}^2 L_c^3}{6EI_c} + \frac{(2.6\alpha_c V_{DC}^2 + N_{DC}^2)L_c r_c^2}{2EI_c}
\end{aligned} \tag{34}
$$

By combining Eqs. (5), (10), and (21), N_{AB} was obtained, and by substitution of this equation, Eq. (2) and Eq. (13) in Eq. (33), the value of strain energy of column AB in Eq. (35) is obtained:

2.2. Calculating strain energy of the beams

Strain energy for beams is calculated under the effect of internal bending moment, internal axial force, and internal shear force. To calculate strain energy in the beams, first, we obtained the equation of internal force changes in beams AD and BC according to Fig. 6c and d, and then, using the general energy equation, we obtained the amount of strain energy stored in the beams. The internal moment values of the beams were obtained by Eqs. (38) and (39):

$$M_{AD}(x) = M_{AD} - V_{AD}x, \quad 0 \le x \le L_b \tag{38}$$

$$M_{BC}(x) = M_{BC} - V_{BC}x, \quad 0 \le x \le L_b \tag{39}$$

Strain energy values due to bending, axial, and shear deformations for beams were calculated by Eq. (40) and Eq. (41). In these equations, E is Young's modulus and G is shear modulus of steel that is obtained in Eq. (27). Also, A_b is the area of beam cross-section, and A_b' is the effective shear area of the beam cross-section obtained in Eq. (29).

$$
\begin{aligned}
U_{AD} &= \frac{1}{2EI_b} \int_0^{L_b} M_{AD}^2(x)dx + \frac{V_{AD}^2 L_b}{2GA_b'} + \frac{N_{AD}^2 L_b}{2EA_b} \\
&= \frac{1}{2EI_b} \int_0^{L_b} (M_{AD} - V_{AD}x)^2 dx + 2.6\alpha_b \frac{V_{AD}^2 L_b}{2EA_b} + \frac{N_{AD}^2 L_b}{2EA_b} \\
&= \frac{M_{AD}^2 L_b}{2EI_b} - \frac{M_{AD}V_{AD}L_b^2}{2EI_b} + \frac{V_{AD}^2 L_b^3}{6EI_b} + \frac{(2.6\alpha_b V_{AD}^2 + N_{AD}^2)L_b r_b^2}{2EI_b}
\end{aligned} \tag{40}
$$

$$
\begin{aligned}
U_{AB} &= \frac{L_c}{6EI_c} \left[3M_A^2 + 3M_A(-M_A - M_B) + (-M_A - M_B)^2 + 3r_c^2 \left(2.6\alpha_c \left(\frac{-M_A - M_B}{L_c} \right)^2 + \left(\frac{M_B - M_C}{L_b} \right)^2 \right) \right] \\
&= \frac{L_c}{6EI_c} \left[M_A^2 - M_A M_B + M_B^2 + \frac{7.8\alpha_c r_c^2}{L_c^2}(M_A^2 + 2M_A M_B + M_B^2) + \frac{3r_c^2}{L_b^2}(M_B^2 - 2M_B M_C + M_C^2) \right]
\end{aligned} \tag{35}
$$

By combining Eq. (9), and Eq. (21), N_{DC} was obtained, and by substitution of this equation, Eq. (8) and Eq. (17) in Eq. (34), the value of strain energy of column DC in Eq. (36) is obtained:

$$
\begin{aligned}
U_{DC} &= \frac{L_c}{6EI_c} \left[3M_D^2 - 3M_D(M_D + M_C) + (M_D + M_C)^2 + 3r_c^2 \left(2.6\alpha_c \left(\frac{M_D + M_C}{L_c} \right)^2 + \left(\frac{M_A - M_D - PL_c}{L_b} \right)^2 \right) \right] \\
&= \frac{L_c}{6EI_c} \left[M_D^2 - M_D M_C + M_C^2 + \frac{7.8\alpha_c r_c^2}{L_c^2}(M_D^2 + 2M_D M_C + M_C^2) + \frac{3r_c^2}{L_b^2}(M_A^2 - 2M_A M_D - 2M_A PL_c + 2M_D PL_c + M_D^2 + P^2 L_c^2) \right]
\end{aligned} \tag{36}
$$

By adding up Eqs. (35) and (36), the total strain energy caused by bending, axial, and shear deformations is calculated for columns:

$$
\begin{aligned}
U_{columns,bav} &= U_{AB} + U_{DC} \\
&= \frac{L_c}{6EI_c} \left[M_A^2 - M_A M_B + M_B^2 + M_D^2 - M_D M_C + M_C^2 + \frac{7.8\alpha_c r_c^2}{L_c^2}(M_A^2 + 2M_A M_B + M_B^2 + M_D^2 + 2M_D M_C + M_C^2) + \frac{3r_c^2}{L_b^2}(M_B^2 - 2M_B M_C + M_C^2 \right. \\
&\quad \left. + M_A^2 - 2M_A M_D - 2M_A PL_c + 2M_D PL_c + M_D^2 + P^2 L_c^2) \right]
\end{aligned} \tag{37}
$$

$$U_{BC} = \frac{1}{2EI_b} \int_0^{L_b} M_{BC}^2(x)dx + \frac{V_{BC}^2 L_b}{2GA_b'} + \frac{N_{BC}^2 L_b}{2EA_b}$$

$$= \frac{1}{2EI_b} \int_0^{L_b} (M_{BC} - V_{BC}x)^2 dx + 2.6\alpha_b \frac{V_{BC}^2 L_b}{2EA_b} + \frac{N_{BC}^2 L_b}{2EA_b}$$

$$= \frac{M_{BC}^2 L_b}{2EI_b} - \frac{M_{BC}V_{BC}L_b^2}{2EI_b} + \frac{V_{BC}^2 L_b^3}{6EI_b} + \frac{(2.6\alpha_b V_{BC}^2 + N_{BC}^2)L_b r_b^2}{2EI_b} \qquad (41)$$

By substitution of Eqs. (2), (8), (22), and (24) in Eq. (40), the strain energy value of beam AD in Eq. (42) is obtained:

$$U_{AD} = \frac{L_b}{6EI_b}\left[3M_A^2 - 3M_A(M_A - M_D) + (M_A - M_D)^2 + 3r_b^2\left(2.6\alpha_b\left(\frac{M_A - M_D}{L_b}\right)^2\right)\right]$$

$$= \frac{L_b}{6EI_b}\left[M_A^2 + M_A M_D + M_D^2 + \frac{7.8\alpha_b r_b^2}{L_b^2}(M_A^2 - 2M_A M_D + M_D^2)\right]$$

$$(42)$$

By substitution of Eqs. (2), (4), (6), (13), and (21) in Eq. (41), the strain energy value of beam BC in Eq. (43) is obtained:

$$U_{BC} = \frac{L_b}{6EI_b}\left[3M_B^2 - 3M_B(M_B - M_C) + (M_B - M_C)^2 + 3r_b^2\left(2.6\alpha_b\left(\frac{M_B - M_C}{L_b}\right)^2 + \left(\frac{M_A + M_B - PL_c}{L_c}\right)^2\right)\right]$$

$$= \frac{L_b}{6EI_b}\left[M_B^2 + M_B M_C + M_C^2 + \frac{7.8\alpha_b r_b^2}{L_b^2}(M_B^2 - 2M_B M_C + M_C^2) + \frac{3r_b^2}{L_c^2}(M_A^2 + 2M_A M_B - 2M_A PL_c - 2M_B PL_c + M_B^2 + P^2 L_c^2)\right]$$

$$(43)$$

By adding up Eqs. (42) and (43), the total strain energy caused by bending, axial, and shear deformations is calculated for beams:

$$U_{beams,bav} = U_{AD} + U_{BC}$$

$$= \frac{L_b}{6EI_b}\left[M_A^2 + M_A M_D + M_D^2 + M_B^2 + M_B M_C + M_C^2 + \frac{7.8\alpha_b r_b^2}{L_b^2}(M_A^2 - 2M_A M_D + M_D^2 + M_B^2 - 2M_B M_C + M_C^2) + \frac{3r_b^2}{L_c^2}(M_A^2 + 2M_A M_B - 2M_A PL_c - 2M_B PL_c + M_B^2 + P^2 L_c^2)\right]$$

$$(44)$$

2.3. Calculating strain energy of the quarter-elliptic brace

Strain energy is calculated under the effect of internal bending moment, internal axial force, and internal shear force for the quarter-elliptic brace. To calculate the strain energy in the quarter-elliptic brace, we first obtained the equation of changes of internal forces in the quarter-elliptic brace AC according to Fig. 7 and the elliptic equation (Eq. (45)), and then, using the general energy equation, we obtained the amount of strain energy stored in the member:

$$\frac{x^2}{a^2} + \frac{y^2}{b^2} = 1 \rightarrow y = b\sqrt{1 - \frac{x^2}{a^2}}, \qquad 0 \leq x \leq a \qquad (45)$$

An infinitesimal arc length (ds) is obtained using Eq. (46) for any desired point in coordinates (x, y):

$$ds = \sqrt{dx^2 + dy^2} = \sqrt{1 + \left(\frac{dy}{dx}\right)^2}dx = \sqrt{1 + y'^2}dx \qquad (46)$$

Using Eq. (45), the inclination angle of the tangent line from each point to the horizontal axis (ϕ) is obtained for the quarter-elliptic bracing member:

$$y' = -b.\frac{\frac{x}{a^2}}{\sqrt{1 - \frac{x^2}{a^2}}} \rightarrow |y'| = tan\phi \qquad (47)$$

According to Eq. (47), and the use of trigonometric identities (Pythagorean identities), $sin\phi$ and $cos\phi$ in terms of × were obtained in Eqs. (48) and (49):

$$cos^2\phi = \frac{1}{1 + tan^2\phi} = \frac{1}{1 + \cfrac{b^2\frac{x^2}{a^4}}{1 - \frac{x^2}{a^2}}}$$

$$= \frac{1 - \frac{x^2}{a^2}}{1 - \frac{x^2}{a^2} + \frac{b^2 x^2}{a^4}} \rightarrow cos\phi = \sqrt{\frac{1 - \frac{x^2}{a^2}}{1 - \frac{x^2}{a^2} + \frac{b^2 x^2}{a^4}}} \qquad (48)$$
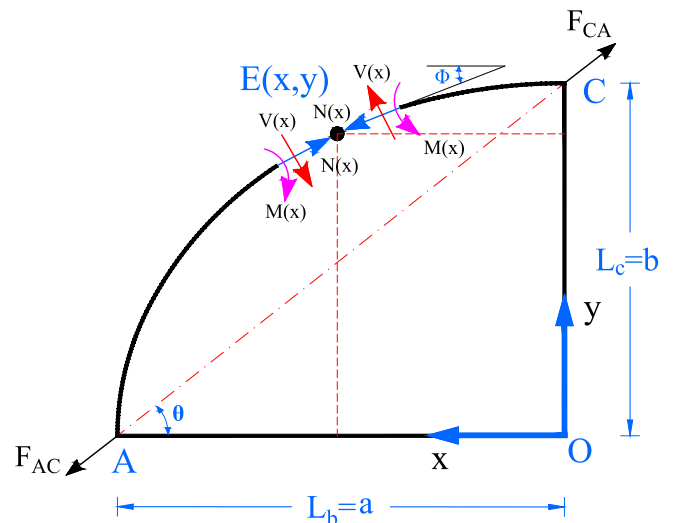

Fig. 7. The internal efforts of the element AC in the quarter-elliptic brace.

$$sin^2\phi = 1 - cos^2\phi = \frac{1 - \frac{x^2}{a^2} + \frac{b^2x^2}{a^4} - 1 + \frac{x^2}{a^2}}{1 - \frac{x^2}{a^2} + \frac{b^2x^2}{a^4}}$$

$$= \frac{\frac{b^2x^2}{a^4}}{1 - \frac{x^2}{a^2} + \frac{b^2x^2}{a^4}} \rightarrow sin\phi = \frac{b\frac{x}{a^2}}{\sqrt{1 - \frac{x^2}{a^2} + \frac{b^2x^2}{a^4}}} \tag{49}$$

Using static equilibrium equations and according to Fig. 7, internal bending, axial, and shear efforts for quarter-elliptic bracing member were calculated in Eqs. (50)–(53):

$$F_{AC} = F_{CA} = F \tag{50}$$

$$\sum F_x = 0 \rightarrow Fcos\theta = N(x)cos\phi + V(x)sin\phi \tag{51}$$

$$\sum F_y = 0 \rightarrow Fsin\theta = N(x)sin\phi - V(x)cos\phi \tag{52}$$

$$\sum M_E = 0 \rightarrow M(x) = Fsin\theta.x$$
$$-Fb\left(1 - \sqrt{1 - \frac{x^2}{a^2}}\right)cos\theta \tag{53}$$

The $sin\theta$ and $cos\theta$ values are dependent on beam length (L_b) and column length (L_c). By solving the system of equations (51) and (52), axial force and shear force of quarter-elliptic bracing member in terms of x were calculated in Eqs. (54) and (55):

$$N(x) = F(cos\theta cos\phi + sin\theta sin\phi) \tag{54}$$

$$V(x) = F(cos\theta sin\phi - sin\theta cos\phi) \tag{55}$$

The strain energy stored in the quarter-elliptic bracing member under the effect of internal bending moment, internal axial force, and internal shear force based on general energy equation and Eq. (46) are as follows:

$$U_{quarter-elliptic\ brace,bav} = U_b + U_a + U_v$$
$$= \int \frac{M(x)^2}{2EI_q}ds + \int \frac{N(x)^2}{2EA_q}ds + \int \frac{V(x)^2}{2GA_q'}ds \tag{56}$$
$$= \int_0^a \frac{M(x)^2}{2EI_q}.\sqrt{1 + y'^2}dx + \int_0^a \frac{N(x)^2}{2EA_q}.\sqrt{1 + y'^2}dx$$
$$+ \int_0^a \frac{V(x)^2}{2GA_q'}.\sqrt{1 + y'^2}dx$$

where:

$$\sqrt{1 + y'^2} = \sqrt{1 + \frac{b^2\frac{x^2}{a^4}}{1 - \frac{x^2}{a^2}}} = \sqrt{\frac{1 - \frac{x^2}{a^2} + b^2\frac{x^2}{a^4}}{1 - \frac{x^2}{a^2}}} \tag{57}$$

In this equation, *E* is Young's modulus, and *G* is shear modulus of steel which is obtained in Eq. (27). Also, A_q is the cross-sectional area of quarter-elliptic brace, and A_q' is the effective shear area of cross-section of the quarter-elliptic brace obtained in Eq. (30). Strain energy was obtained under the effect of internal bending moment in quarter-elliptic bracing member by inserting Eqs. (1), (53), and (57) in the first term of Eq. (56):

$$U_b = \frac{F^2}{2EI_q}\int_0^a \left[sin\theta.x - bcos\theta.\left(1 - \sqrt{1 - \frac{x^2}{a^2}}\right)\right]^2 \times \frac{\sqrt{1 - \frac{x^2}{a^2} + b^2\frac{x^2}{a^4}}}{\sqrt{1 - \frac{x^2}{a^2}}}dx$$

$$= \frac{F^2b^2}{2EI_q.(1 + e^2)}\int_0^a \left[\frac{x}{a} - \left(1 - \sqrt{1 - \frac{x^2}{a^2}}\right)\right]^2 \times \frac{\sqrt{1 - \frac{x^2}{a^2} + e^2\frac{x^2}{a^2}}}{\sqrt{1 - \frac{x^2}{a^2}}}dx \tag{58}$$

To solve integrals in Eq. (58), variable substitution (variable change) based on Eq. (59) was used:

$$t = \frac{x}{a} \rightarrow dt = \frac{dx}{a} \rightarrow dx = a.dt \tag{59}$$

By inserting Eq. (59) in Eq. (58), we can conclude:

$$U_b = \frac{F^2b^2a}{2EI_q}\int_0^1 \frac{\left[t - 1 + \sqrt{1 - t^2}\right]^2.\sqrt{1 + (e^2 - 1).t^2}}{(1 + e^2).\sqrt{1 - t^2}}dt \tag{60}$$

If:

$$\lambda_b(e) = \int_0^1 \frac{\left[t - 1 + \sqrt{1 - t^2}\right]^2.\sqrt{1 + (e^2 - 1).t^2}}{(1 + e^2).\sqrt{1 - t^2}}dt \tag{61}$$

Then, the strain energy under the effect of internal bending moment in the quarter-elliptic bracing member is equal to:

$$U_b = \frac{F^2ab^2}{2EI_q}.\lambda_b(e) \tag{62}$$

$\lambda_b(e)$ is a function in terms of *e* (the ratio of column length to beam length) that can be calculated numerically. The $\lambda_b(e)$ value for different values of *e* is graphically shown in Fig. 8a. Strain energy was obtained under the effect of internal axial force in quarter-elliptic bracing member by inserting Eqs. (1), (54), and (57) in the second term of Eq. (56):

$$U_a = \frac{F^2}{2EA_q}\int_0^a \left[cos\theta cos\phi + sin\theta sin\phi\right]^2 \times \frac{\sqrt{1 - \frac{x^2}{a^2} + e^2\frac{x^2}{a^2}}}{\sqrt{1 - \frac{x^2}{a^2}}}dx$$

$$= \frac{F^2}{2EA_q}\int_0^a \left[\frac{1}{\sqrt{1 + e^2}}.\frac{\sqrt{1 - \frac{x^2}{a^2}}}{\sqrt{1 - \frac{x^2}{a^2} + e^2\frac{x^2}{a^2}}} + \frac{e}{\sqrt{1 + e^2}}.\frac{e\frac{x}{a}}{\sqrt{1 - \frac{x^2}{a^2} + e^2\frac{x^2}{a^2}}}\right]^2$$
$$\times \frac{\sqrt{1 - \frac{x^2}{a^2} + e^2\frac{x^2}{a^2}}}{\sqrt{1 - \frac{x^2}{a^2}}}dx \tag{63}$$

To solve integrals in Eq. (63), variable substitution (variable change) based on Eq. (59) was used. By inserting Eq. (59) in Eq. (63), we can conclude:

$$U_a = \frac{F^2a}{2EA_q}.\int_0^1 \frac{1}{(1 + e^2)}.\frac{\left[\sqrt{1 - t^2} + e^2t\right]^2}{\sqrt{(1 - t^2).[1 + (e^2 - 1)t^2]}}dt \tag{64}$$

If:

$$\lambda_a(e) = \int_0^1 \frac{1}{(1 + e^2)}.\frac{\left[\sqrt{1 - t^2} + e^2t\right]^2}{\sqrt{(1 - t^2).[1 + (e^2 - 1)t^2]}}dt \tag{65}$$

Then, the strain energy under the effect of internal axial force in the quarter-elliptic bracing member is equal to:

$$U_a = \frac{F^2a}{2EA_q}.\lambda_a(e) \tag{66}$$

$\lambda_a(e)$ is a function in terms of *e* (the ratio of column length to beam length) that can be calculated numerically. The $\lambda_a(e)$ value for different values of *e* is graphically shown in Fig. 8a. Strain energy was obtained under the effect of internal shear force in quarter-elliptic bracing member by inserting Eqs. (1), (55), and (57) in the third term of Eq. (56):
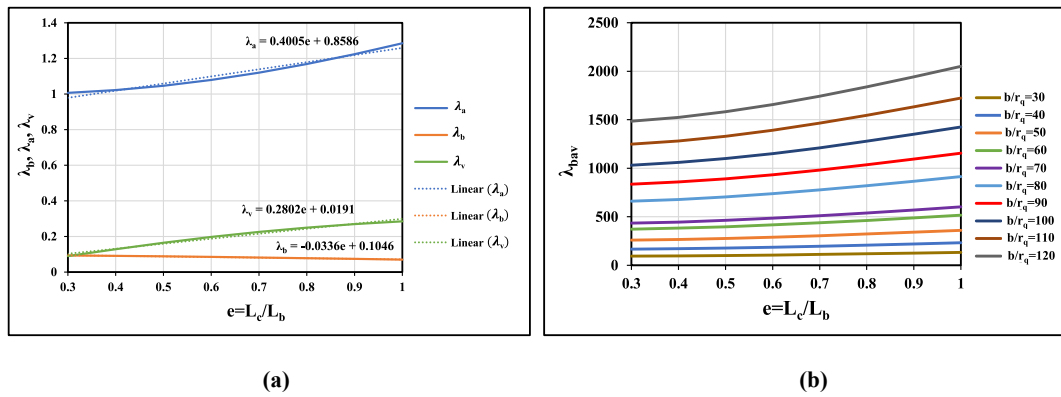
Fig. 8. (a) The $\lambda_b(e), \lambda_a(e)$, and $\lambda_v(e)$ parameters as a function of parameter e, (b) $\lambda_{bav}(e)$ as a function of parameter e assuming constant $\alpha_q = 2$.

$$U_v = \frac{\alpha_q.F^2}{2GA_q} \int_0^a [cos\theta sin\phi - sin\theta cos\phi]^2 \times \frac{\sqrt{1 - \frac{x^2}{a^2} + e^2\frac{x^2}{a^2}}}{\sqrt{1 - \frac{x^2}{a^2}}} dx$$

$$= \alpha_q.\frac{F^2}{2GA_q} \int_0^a \left[\frac{1}{\sqrt{1+e^2}} . \frac{e.\frac{x}{a}}{\sqrt{1 - \frac{x^2}{a^2} + e^2\frac{x^2}{a^2}}} - \frac{e}{\sqrt{1+e^2}} . \frac{\sqrt{1 - \frac{x^2}{a^2}}}{\sqrt{1 - \frac{x^2}{a^2} + e^2\frac{x^2}{a^2}}} \right]^2$$

$$\times \frac{\sqrt{1 - \frac{x^2}{a^2} + e^2\frac{x^2}{a^2}}}{\sqrt{1 - \frac{x^2}{a^2}}} dx$$

(67)

To solve integrals in Eq. (67), variable substitution (variable change) based on Eq. (59) was used. By inserting Eq. (59) in Eq. (67), we can conclude:

$$U_v = \alpha_q.\frac{F^2 a}{2GA_q} . \int_0^1 \frac{e^2}{(1+e^2)} . \frac{\left[t - \sqrt{1-t^2} \right]^2}{\sqrt{(1-t^2).[1 + (e^2 - 1)t^2]}} dt$$

(68)

stored in the quarter-elliptic brace is simplified by inserting Eqs. (62), (66), and (70) in Eq. (56) as follows:

$$U_{quarter-elliptic\ brace,bav} = U_b + U_a + U_v$$
$$= \frac{F^2 ab^2}{2EI_q}.\lambda_b(e) + \frac{F^2 a}{2EA_q}.\lambda_a(e) + \alpha_q.\frac{F^2.a}{2GA_q}.\lambda_v(e)$$
$$= \frac{F^2.a}{2EA_q}\left[\left(\frac{b}{r_q}\right)^2.\lambda_b + \lambda_a + 2.6\alpha_q\lambda_v \right] = \frac{F^2.a}{2EA_q}.\frac{\lambda_{bav}}{1+e^2}$$

(71)

where:

$$\lambda_{bav} = \left[\left(\frac{b}{r_q}\right)^2.\lambda_b + \lambda_a + 2.6\alpha_q\lambda_v \right].(1+e^2)$$

(72)

$\lambda_{bav}(e)$ is a function in terms of e (the ratio of column length to beam length) that can be calculated numerically. The $\lambda_{bav}(e)$ value for different values of e is graphically shown in Fig. 8b considering the shear shape coefficient of the cross-section of the quarter-elliptic brace equal to 2 (BOX sections). With fitting curves λ_b, λ_a and λ_v using linear regression in Fig. 8a and inserting obtained linear equations in Eq. (72), the $\lambda_{bav}(e)$ value is equal to

$$\lambda_{bav} = \left[\left(\frac{b}{r_q}\right)^2 \times (-0.0336e + 0.1046) + (0.4005e + 0.8586) + 2.6\alpha_q.(0.2802e + 0.0191) \right]$$
$$\times (1 + e^2)$$

(73)

If:

$$\lambda_v(e) = \int_0^1 \frac{e^2}{(1+e^2)} . \frac{\left[t - \sqrt{1-t^2} \right]^2}{\sqrt{(1-t^2).[1 + (e^2 - 1)t^2]}} dt$$

(69)

Then, the strain energy under the effect of internal shear force in the quarter-elliptic bracing member is equal to:

$$U_v = \alpha_q.\frac{F^2.a}{2GA_q}.\lambda_v(e)$$

(70)

$\lambda_v(e)$ is a function in terms of e (the ratio of column length to beam length) that can be calculated numerically. The $\lambda_v(e)$ value for different values of e is graphically shown in Fig. 8a. The amount of strain energy

The amount of strain energy stored in quarter-elliptic brace is calculated by inserting Eqs. (1) and (26) in Eq. (71) as follows:

$$U_{quarter-elliptic\ brace,bav} = \frac{a.\lambda_{bav}}{2EA_q L_c^2}$$
$$\times (PL_c - M_A - M_B + M_C + M_D)^2$$

(74)

2.4. Strain energy of the QEB-MFs

By adding strain energy (caused by bending, axial, and shear deformations) of columns, beams, and quarter-elliptic bracing member according to Eqs. (37), (44), and (74), strain energy of steel moment frame equipped with quarter-elliptic brace is obtained as follows:

$$U = U_{columns,bav} + U_{beams,bav} + U_{quarter-elliptic\ brace,bav}$$

$$= R.\big(M_A^2 - M_A M_B + M_B^2 + M_D^2 - M_D M_C + M_C^2 + \kappa_c.\big(M_A^2 + 2M_A M_B + M_B^2 + M_D^2 + 2M_D M_C + M_C^2\big) + \mu_c.\big(M_B^2 - 2M_B M_C + M_C^2 + M_A^2 - 2M_A M_D - 2M_A PL_c$$

$$+2M_D PL_c + M_D^2 + P^2 L_c^2\big)\big) + S.\big(M_A^2 + M_A M_D + M_D^2 + M_B^2 + M_B M_C + M_C^2 + \kappa_b.\big(M_A^2 - 2M_A M_D + M_D^2 + M_B^2 - 2M_B M_C + M_C^2\big) + \mu_b.\big(M_A^2 + 2M_A M_B - 2M_A PL_c$$

$$- 2M_B PL_c + M_B^2 + P^2 L_c^2\big)\big) + T.(PL_c - M_A - M_B + M_C + M_D)^2$$

$$(75)$$

In this equation, R, κ_c, and μ_c are modification coefficients for simplification of strain energy of columns; S, κ_b, and μ_b are modification coefficients for simplification of strain energy of beams; and T is the modification coefficient for simplification of strain energy of quarter-elliptic bracing member, which are equal to:

$$R = \frac{L_c}{6EI_c}, \quad \kappa_c = \frac{7.8\alpha_c r_c^2}{L_c^2}, \quad \mu_c = \frac{3r_c^2}{L_b^2} \tag{76}$$

$$S = \frac{L_b}{6EI_b}, \quad \kappa_b = \frac{7.8\alpha_b r_b^2}{L_b^2}, \quad \mu_b = \frac{3r_b^2}{L_c^2} \tag{77}$$

$$T = \frac{a.\lambda_{bav}}{2EA_q L_c^2} \tag{78}$$

Based on Castigliano's second theorem, in a structure with linear elastic behavior, in the absence of temperature change and support settlement, if we have the stored strain energy in terms of the effective forces of the node or the concentrated moments of the node on that structure, the partial derivative of the strain energy function will be equal to the displacement along that force in the structure compared to any of the effective forces involved in the structure. Also, the partial derivative of energy function in relation to each concentrated moment imposed on the structure is equal to the corresponding rotation of that moment in the main structure [36]. According to this theorem and Eq. (75) in nodes A, B, C, and D, it is as below:

By solving the system of equations (79) to (82), unknown moments M_A, M_B, M_C, and M_D with a good approximation are equal to the following values:

$$M_A = M_B \approx \eta P \tag{83}$$

$$M_C = M_D \approx -\eta P \tag{84}$$

In these equations:

$$\eta = \frac{2L_c(\mu_c R + \mu_b S + T)}{R(1 + 4\kappa_c + 4\mu_c) + S(1 + 4\kappa_b + 4\mu_b) + 8T} \tag{85}$$

κ_c and μ_c are the modification coefficients for considering the effects of shear deformations and axial deformation of columns, respectively; and κ_b and μ_b are modification coefficients for considering the effects of shear deformation and axial deformation of beams, respectively. If $\kappa_c + \mu_c \approx \kappa_c$ and $\kappa_b + \mu_b \approx \kappa_b$, then by simplifying Eq. (85), it is as below:

$$\eta = \frac{2L_c(\mu_c R + \mu_b S + T)}{R(1 + 4\kappa_c) + S(1 + 4\kappa_b) + 8T} \tag{86}$$

By inserting Eqs. (83) and (84) in Eq. (75), the strain energy of the steel moment frame equipped with quarter-elliptic brace is obtained as follows:

$$U = R.\big(2\eta^2 P^2 + 8\kappa_c \eta^2 P^2 + \mu_c.\big(8\eta^2 P^2 - 4\eta P^2 L_c + P^2 L_c^2\big)\big)$$

$$+S.\big(2\eta^2 P^2 + 8\kappa_b \eta^2 P^2 + \mu_b.\big(4\eta^2 P^2 - 4\eta P^2 L_c + P^2 L_c^2\big)\big) + T.(PL_c - 4\eta P)^2 \tag{87}$$

$$\Delta\theta_A = \frac{\partial U}{\partial M_A} = 0$$

$$\rightarrow R.(2M_A - M_B + \kappa_c.(2M_A + 2M_B) + \mu_c.(2M_A - 2M_D - 2PL_c)) + S.(2M_A + M_D + \kappa_b.(2M_A - 2M_D) + \mu_b.(2M_A + 2M_B - 2PL_c)) + 2T.(M_A + M_B - M_C - M_D - PL_c) = 0 \tag{79}$$

$$\Delta\theta_B = \frac{\partial U}{\partial M_B} = 0$$

$$\rightarrow R.(2M_B - M_A + \kappa_c.(2M_B + 2M_A) + \mu_c.(2M_B - 2M_C)) + S.(2M_B + M_C + \kappa_b.(2M_B - 2M_C) + \mu_b.(2M_B + 2M_A - 2PL_c)) + 2T.(M_A + M_B - M_C - M_D - PL_c) = 0 \tag{80}$$

$$\Delta\theta_C = \frac{\partial U}{\partial M_C} = 0$$

$$\rightarrow R.(2M_C - M_D + \kappa_c.(2M_C + 2M_D) + \mu_c.(2M_C - 2M_C)) + S.(2M_C + M_B + \kappa_b.(2M_C - 2M_B)) + 2T.(PL_c - M_A - M_B + M_C + M_D) = 0 \tag{81}$$

$$\Delta\theta_D = \frac{\partial U}{\partial M_D} = 0$$

$$\rightarrow R.(2M_D - M_C + \kappa_c.(2M_D + 2M_C) + \mu_c.(2M_D - 2M_A + 2PL_c)) + S.(2M_D + M_A + \kappa_b.(2M_D - 2M_A)) + 2T.(PL_c - M_A - M_B + M_C + M_D) = 0 \tag{82}$$

To calculate the stiffness of the frame, first, using Castigliano's second theorem and according to Eq. (87), the horizontal displacement of the frame (Δ_{Cx}) is calculated as follows:

$$\Delta_{Cx} = \frac{\partial U}{\partial P}$$
$$= R.\left(4\eta^2 P + 16\kappa_c \eta^2 P + \mu_c.\left(16\eta^2 P - 8\eta PL_c + 2PL_c^2\right)\right)$$
$$+S.\left(4\eta^2 P + 16\kappa_b \eta^2 P + \mu_b.\left(8\eta^2 P - 8\eta PL_c + 2PL_c^2\right)\right) + T.\left(2PL_c{}^2 - 16\eta PL_c + 32\eta^2 P\right) \tag{88}$$

By inserting Eq. (86) in Eq. (88), it is as below:

$$\Delta_{Cx} = \frac{32PL_c^2(\mu_c R + \mu_b S + T)}{(4\kappa_c R + 4\kappa_b S + R + S + 8T)^2}$$
$$\times \left[\left(2\mu_c^2 + \left(\kappa_c + \frac{1}{4}\right)^2\right)R^2 + \left(\left(3\mu_b \mu_c + 2\left(\kappa_c + \frac{1}{4}\right)\left(\kappa_b + \frac{1}{4}\right)\right)S + 2\left(\kappa_c + \mu_b + \frac{1}{4}\right)T\right)R + \left(\left(\mu_b^2 + \left(\kappa_b + \frac{1}{4}\right)^2\right)S + 2\left(\kappa_b + \frac{1}{2}\mu_b + \frac{1}{4}\right)T\right)S\right] \tag{89}$$

If $\kappa_c + \mu_c \approx \kappa_c$, $\kappa_b + \mu_b \approx \kappa_b$, and $\mu_c^2 = \mu_b^2 = \mu_b \mu_c \approx 0$, then by simplifying Eq. (89), it is as below:

$$\Delta_{Cx} = 2PL_c^2\left(\frac{(4\kappa_c R + 4\kappa_b S + R + S)(\mu_c R + \mu_b S + T)}{R(1 + 4\kappa_c) + S(1 + 4\kappa_b) + 8T}\right) \tag{90}$$

Then, the elastic stiffness of the steel moment frame equipped with quarter-elliptic brace under lateral load of P according to Eq. (90) is obtained as follows:

$$K = \frac{P}{\Delta C_x} = \frac{R(1 + 4\kappa_c) + S(1 + 4\kappa_b) + 8T}{2L_c(4\kappa_c R + 4\kappa_b S + R + S)(\mu_c R + \mu_b S + T)} \tag{91}$$

To simplify the stiffness equation, two parameters β and γ are introduced, and their values according to Eqs. (77) and (78) are as follows:

$$\beta = \frac{I_b}{I_c} \tag{92}$$

$$\gamma = \frac{T}{S} = \frac{\frac{a.\lambda_{bav}}{2EA_q L_c^2}}{\frac{L_b}{6EI_b}} = \frac{3I_b \lambda_{bav}}{A_q L_c^2} \tag{93}$$

Also, the ratio of parameter R to parameter S according to Eqs. (76) and (77) and placement of Eqs. (1) and (92) in these equations is equal to:

$$\frac{R}{S} = \frac{\frac{L_c}{6EI_c}}{\frac{L_b}{6EI_b}} = \frac{L_c}{L_b} \times \frac{I_b}{I_c} = e\beta \tag{94}$$

By factoring the S parameter from the numerator and denominator of Eq. (91) and placement of Eqs. (78), (93), and (94) in this equation, the final stiffness value is obtained as follows:

$$K = \frac{\left(\frac{R}{S}\right)(1 + 4\kappa_c) + (1 + 4\kappa_b) + 8\left(\frac{T}{S}\right)}{2SL_c^2\left(4\kappa_c\left(\frac{R}{S}\right) + 4\kappa_b + \left(\frac{R}{S}\right) + 1\right)\left(\mu_c\left(\frac{R}{S}\right) + \mu_b + \left(\frac{T}{S}\right)\right)} \tag{95}$$

$$\rightarrow K = \frac{EA_q\gamma((e\beta)(1 + 4\kappa_c) + (1 + 4\kappa_b) + 8\gamma)}{L_b.\lambda_{bav}((e\beta)(1 + 4\kappa_c) + (1 + 4\kappa_b))(\mu_c(e\beta) + \mu_b + \gamma)}$$

By simplifying Eq. (95) by Eqs. (1), (92), and (93), it is as below:

$$K = K_{frame,bav} + K_{brace,bav}$$
$$= \frac{24EI_c}{L_c^3}\left(\frac{e\beta}{(e\beta + 1 + 4\kappa_c(e\beta) + 4\kappa_b)\left(\frac{\mu_c(e\beta) + \mu_b}{\gamma} + 1\right)}\right) + \frac{EA_q\gamma}{L_b.\lambda_{bav}(\mu_c(e\beta) + \mu_b + \gamma)} \tag{96}$$

In this equation, the first term is the stiffness of the steel moment frame considering bending, shear, and axial deformations, and the second term is the stiffness of the quarter-elliptic brace considering bending, shear, and axial deformations. If the effect of axial deformations and shear deformations on the beams and columns of the steel moment frame is negligible ($\kappa_c = \kappa_b = \mu_c = \mu_b = 0$), then the elastic stiffness of the steel moment frame equipped with quarter-elliptic brace according to Eq. (95) is equal to:
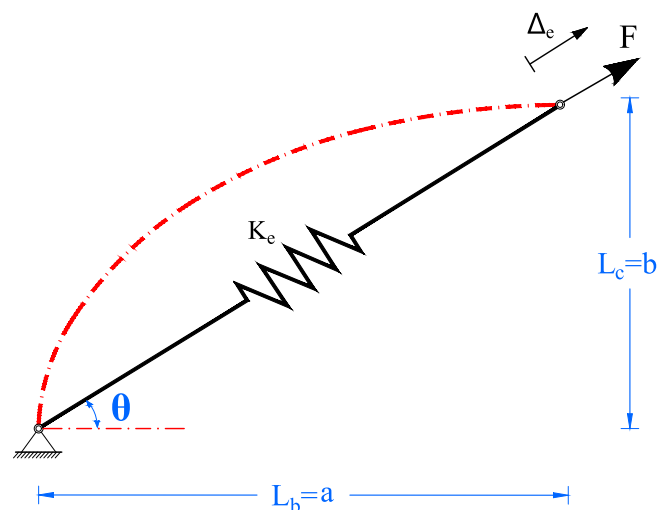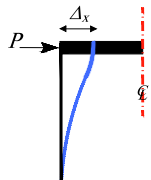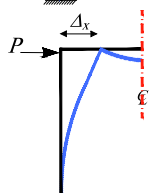
Fig. 9. The equivalent element for the quarter-elliptic brace.

Table 1

Special cases of elastic lateral stiffness in QEB-MF systems.

Case	Beam condition	Deflected shape	Lateral stiffness
a	Rigid beam		$K = \dfrac{1}{m_1}\left[(n_1 + 1)\left(\dfrac{12EI_c}{L_c^3}\right) + n_2\left(\dfrac{EA_q}{L_b . \lambda_{bav}}\right) \right]$
b	Elastic beam*		$K = n_1\left(\dfrac{24EI_c}{L_c^3}\left(\dfrac{e\beta}{1 + e\beta}\right) \right) + n_2\left(\dfrac{EA_q}{L_b . \lambda_{bav}}\right)$

* For single-story and even-span $\left(n_1 = 2^N\right)$ frames.

$$K = \frac{EA_q(e\beta + 1 + 8\gamma)}{L_b . \lambda_{bav}(e\beta + 1)} \tag{97}$$

By simplifying Eq. (97) by Eqs. (1), (92), and (93), it is as below:

$$K = K_{frame,b} + K_{brace,bav} = \frac{24EI_c}{L_c^3}\left(\frac{e\beta}{1 + e\beta}\right) + \frac{EA_q}{L_b . \lambda_{bav}} \tag{98}$$

To obtain normalized stiffness (dimensionless stiffness), the parameter ρ is introduced, which according to Eq. (97) is equal to:

$$\rho\left(e, \beta, \gamma, \frac{b}{r_q}, \alpha_q\right) = \frac{K}{\frac{EA_q}{L_b}} = \frac{e\beta + 1 + 8\gamma}{\lambda_{bav}(e\beta + 1)} \tag{99}$$

Consequently, by having the geometric specifications of column, beams and quarter-elliptic bracing member cross-sections and having material properties, the stiffness of steel moment frame equipped with quarter-elliptic brace under lateral load can be calculated through Eq. (96) with a new and quite accurate method. The calculation steps are as follows:

- Calculation of e (the ratio of column length to beam length) according to Eq. (1).
- Calculation of β (the ratio of moment of inertia of strong axis of beam to moment of inertia of strong axis of column) according to Eq. (92).
- Calculation of γ (ratio of modification coefficients of quarter-elliptic brace member to beams) according to Eq. (93).

- Calculation of λ_{bav} according to Eq. (73) or Fig. 8b.
- Calculation of modification coefficients κ_c and μ_c by inserting the columns specifications in Eq. (76).
- Calculation of modification coefficients κ_b and μ_b by inserting beam specifications in Eq. (77).
- Calculation of elastic stiffness of steel moment frame equipped with quarter-elliptic brace according to Eq. (96).

2.5. Calculation of elastic lateral stiffness of quarter-elliptic-braced steel simple frames (QEB-SFs)

This method can also be used to calculate the elastic lateral stiffness of the simple frame equipped with quarter-elliptic brace (QEB-SF). To this end, first, the axial stiffness of an element equivalent to the quarter-elliptic bracing member under the axial force of F was calculated according to Fig. 9. Then, using this equation and the concepts of spring modeling, the stiffness of the quarter-elliptic brace under lateral force was calculated.

According to Eq. (71), strain energy stored in the quarter-elliptic brace is calculated as follows:

$$U_{quarter-elliptic\ brace,bav} = \frac{F^2 . a}{2EA_q} . \frac{\lambda_{bav}}{1 + e^2} \tag{100}$$

To calculate the stiffness of the element equivalent to the quarter-elliptic bracing member, first, using Castigliano's second theorem and according to Eq. (100), axial displacement (Δ_e) is obtained as follows:

$$\Delta_e = \frac{\partial U}{\partial F} = \frac{F . a}{EA_q} . \frac{\lambda_{bav}}{1 + e^2} \tag{101}$$

Then, according to Eqs. (1) and (101), the elastic axial stiffness of the element equivalent to the quarter-elliptic bracing member under axial force of F is obtained as follows:

$$K_e = \frac{F}{\Delta_e} = \frac{EA_q(1 + e^2)}{L_b . \lambda_{bav}} \tag{102}$$

If we have a two-dimensional single-span and single-story simple frame equipped with quarter-elliptic brace under lateral force, the elastic lateral stiffness of this brace frame using Eq. (1), Eq. (102), and spring modeling concepts is equal to as below:

$$K = K_e cos^2\theta = \frac{EA_q}{L_b . \lambda_{bav}} \tag{103}$$

Consequently, by having the geometric specifications of column, beams, and quarter-elliptic bracing member cross-sections and having material properties, the elastic lateral stiffness of the simple frame equipped with quarter-elliptic brace under the lateral load can be calculated through Eq. (103) with a new method precisely.
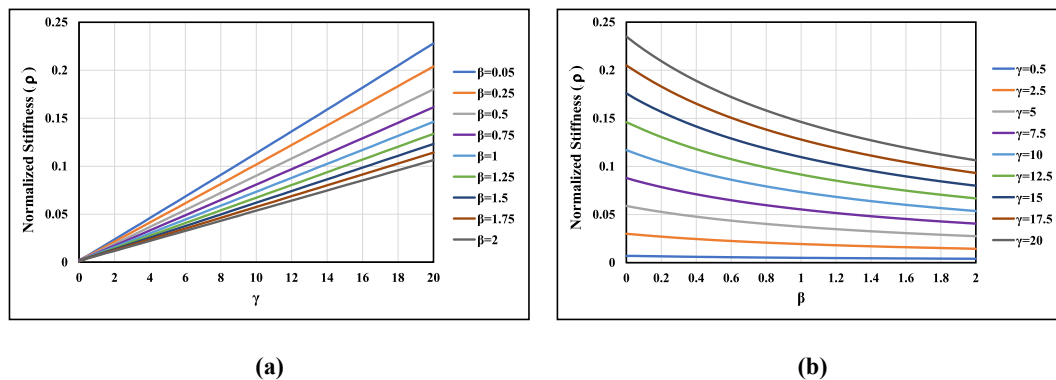

Fig. 10. The changes in normalized stiffness of the QEB-MF system (ρ); (a) versus parameter γ for different values of β, (b) versus parameter β for different values of γ.
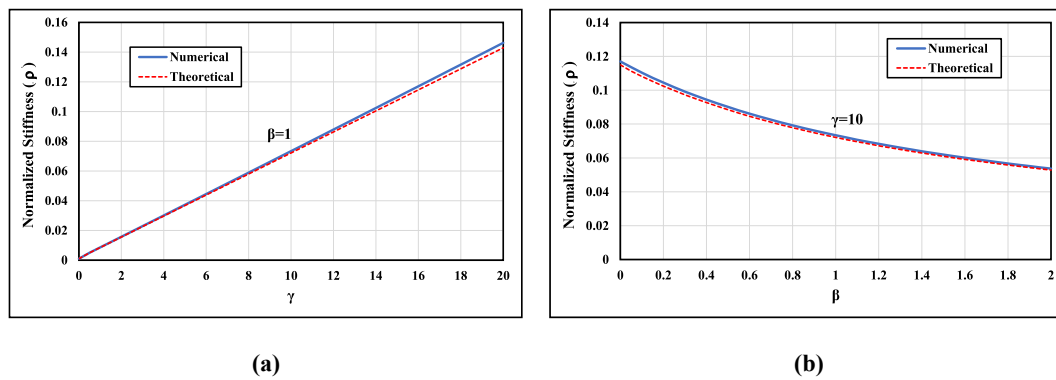
Fig. 11. Comparison of the results obtained by the numerical models and Eq. (99) for ρ; (a) versus parameter γ assuming constant $\beta = 1$, (b) versus parameter β assuming constant $\gamma = 10$.

2.6. Developing the proposed formulation for special cases of the QEB-MF systems

The elastic stiffness of a two-dimensional single-span and single-story QEB-MF system under lateral force, *P*, is obtained in Eq. (98) by assuming the effect of shear and axial deformations to be insignificant on the beams and columns of a steel moment frame. In order to develop this formulation in structural frames, we consider two different conditions for the beams of the moment frame. In the first condition, we consider all of the moment frame system's beams to be rigid ($\beta = I_b/I_c = \infty$); and in the second condition, we consider all of the moment frame's beams to be elastic.

- In the first case, if we have a QEB-MF system with n_1 spans, in which n_2 spans are equipped with quarter-elliptic brace, and also the system has m_1 stories, then its lateral stiffness can be accurately calculated from the equation in Table 1(a) under the force *P*, which is applied to the highest story, in a condition in which all the beams are assumed to be a rigid element with infinite bending stiffness. In this case, all of the columns' support is rigid, and there is no rotation in the connection zone of beams and columns; as a result, in this special case, each column behaves like a beam that has fixed support at one end and sliding support at the other end with the stiffness of $\frac{12EI_c}{L_c^3}$. In this case, the lateral force is divided between the columns and quarter-elliptic braces, and according to the modeling concepts of springs, they act like parallel springs, and their lateral stiffness is added together because they have equal deformations. Also, the stories' lateral stiffnesses are combined like series springs according to the concepts of spring modeling.
- In the second case, if we have a QEB-MF system with n_1 spans ($n_1 = 2^N$), in which n_2 spans are equipped with quarter-elliptic brace, then
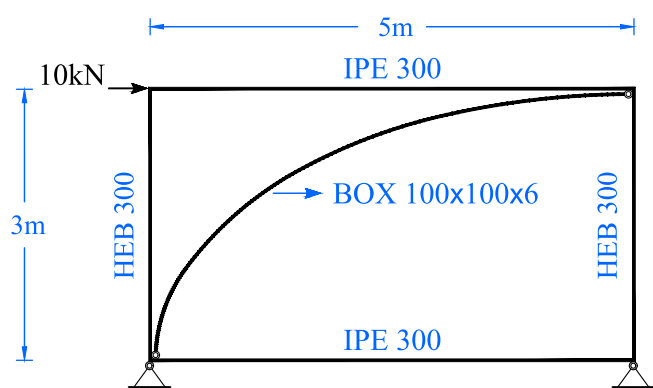
Table 2
Section properties.

Section properties	HEB 300	IPE 300	BOX 100 × 100 × 6
A (mm^2)	14,900	5380	2256
I_x (mm^4)	2517×10^5	836×10^5	33.36×10^5
r_x (mm)	130	125	38.45
$\alpha = A/A'$	4.25	2.48	2

Table 3
Material properties.

Standard and Steel grade	$t \leq 40mm$			
	$F_y[N/mm^2]$	$F_u[N/mm^2]$	$E[N/mm^2]$	ν
S235JR	235	360	210,000	0.3

its lateral stiffness can be accurately calculated from the equation in Table 1(b) under the force *P*, which is applied to the highest story, in a condition that all the beams are assumed to be an elastic element. In this case, the lateral force is divided between the moment frame and the quarter-elliptic braces, and they act like parallel springs, and their lateral stiffness is added together according to the concepts of spring modeling because they have equal deformations.

3. Accuracy verification of QEB-MFs elastic stiffness formulation by finite element modeling

To control and verify the accuracy of elastic stiffness formulation obtained by the strain energy concept and Castigliano's theorem, 1600 two-dimensional single-span and single-story steel moment frames equipped with quarter-elliptic brace under lateral force of 10,000*N* were modeled in OpenSees [37]. The length of columns and the length of beams were considered 3000 *mm* and 5000 *mm*, respectively, and the area and moment of inertia of bending axis (strong axis) of quarter-elliptic bracing member were considered 2256 mm^2 and 33.35×10^5 mm^4, respectively. For all members of frames, the elastic beam-column element was used. Elastic uniaxial materials were used to simulate the behavior of steel in all frames. Using MATLAB programming code, 40 different values for the ratio of moment of inertia of strong axis of beam to moment of inertia of strong axis of column (β) according to Eq. (92) and 40 different values for the ratio of modification coefficients of quarter-elliptic brace member to beams (γ) according to Eq. (93) are assigned to the model made in OpenSees software, and the displacement of 1600 QEB-MF systems was obtained. Then, using the stiffness relation and considering the lateral force of 10,000 *N*, the elastic stiffness of these frames was calculated.

In Fig. 10a, diagrams of normalized stiffness variations (ρ) of QEB-

Fig. 12. Modelling of the two-dimensional single-story single-span QEB-MF.
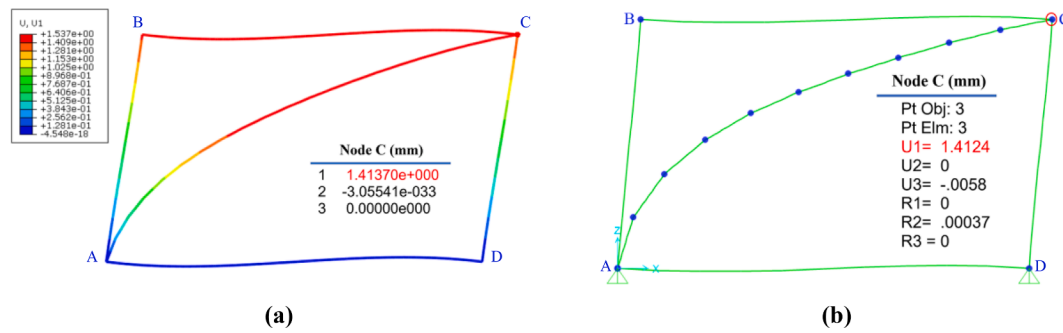
Fig. 13. Elastic displacement of frame subjected to lateral force; (a) Abaqus, (b) SAP2000.

Table 4
Lateral stiffness QEB-MF using the proposed formulation.

No.	Equation or Figure number	Parameters	Calculation of the parameter(s)
1	Eq. (1)	e	0.6
2	Eq. (92)	β	0.332
3	Eq. (93)	γ	8.66
4	Eq. (76)	κ_c and μ_c	$\kappa_c = 0.0622$ $\mu_c = 0.002$
5	Eq. (77)	κ_b and μ_b	$\kappa_b = 0.0121$ $\mu_b = 0.0052$
6	Eqs. (61), (65) and. (69) or Fig. 8a	$\lambda_b(e), \lambda_a(e)$ and $\lambda_v(e)$	$\lambda_b(e) = 0.0852$ $\lambda_a(e) = 1.079064$ $\lambda_v(e) = 0.197287$
7	Eq. (73) or Fig. 8b	$\lambda_{bav}(e)$	701.91
8	Eq. (95)	K	$6990.48 N/mm^2$

MF system versus different values of γ and for different values of β are shown. Because of the fact that the software can not consider the shear shape coefficient of the quarter-elliptic brace section (α_q) due to using elastic beam-column elements, this value is considered to be zero. These diagrams are drawn for 40 different values for γ between 0.5 and 20, and 40 different values for β between 0.05 and 2. For easier evaluation, in Fig. 10a only 9 diagrams of 40 diagrams related to different values of β between 0.05 and 2 were drawn. According to Fig. 10a, changes in normalized stiffness (ρ) of QEB-MF system versus different values of γ and β are linear, and it increases as γ increases.

In Fig. 10b, diagrams of normalized stiffness changes of (ρ) of QEB-MF system versus different values of β and for different values of γ is shown. These diagrams are drawn by assuming the shear shape coefficient of the quarter-elliptic brace cross-section (α_q) equal to zero and for 40 different values for γ between 0.5 and 20, and 40 different values for β between 0.05 and 2. For easier evaluation, in Fig. 10b only 9 diagrams of 40 diagrams related to different values of γ between 0.05 and 2 were drawn. According to Fig. 10b, changes in the normalized stiffness (ρ) of QEB-MF system was reduced as the moment of inertia of strong axis of beam to moment of inertia of strong axis of column (increase of β)

decreased.

Assuming β equal to 1, the normalized stiffness changes (ρ) of QEB-MF system for 40 different values of γ between 0.5 and 20 were calculated through Eq. (99) and its diagram was drawn in Fig. 11a. This diagram was also drawn by assuming the shear shape coefficient of the quarter-elliptic brace cross-section (α_q) equal to zero in Eq. (73). Assuming γ to be 10, the normalized stiffness changes (ρ) of QEB-MF system for 40 different values β between 0.05 and 2 were calculated by Eq. (99), and its diagram is drawn in Fig. 11b. This diagram is also drawn by assuming the shear shape coefficient of the quarter-elliptic brace cross-section (α_q) equal to zero in Eq. (73). According to Fig. 11, the error percentage between the results obtained from the proposed relation and those obtained from numerical analysis of finite elements is tiny, so it can be neglected.

4. Numerical example for calculating elastic stiffness of QEB-MF system

In this section, the accuracy of the proposed relation for calculating the lateral stiffness of QEB-MF system is investigated and verified by a numerical example. For this purpose, a two-dimensional single-span and single-story QEB-MF system is modeled by SAP2000 software and Abaqus software [38]. In this frame, the length of the columns and the length of the beams are 3,000 mm and 5,000 mm, respectively, and this frame is considered under the lateral force of 10,000 N according to Fig. 12.

HEB 300, IPE 300, and BOX 100 × 100 × 6 cross-sections were used for columns, beams, and quarter-elliptic bracing member, respectively, in this frame, the properties of which are presented in Table 2. In this table, A is the area of the cross-section, and I_x and r_x the moment of inertia and the radius of gyration of the cross-section about the bending axis (strong axis), respectively, and α the shear shape coefficient of the cross-section.

For better modeling of quarter-elliptic bracing member in SAP2000 software, this member was divided into ten equal parts. The chosen element for the modeling all frame members in the Abaqus software was element B21 (beam element), which is a 2D element with two nodes,
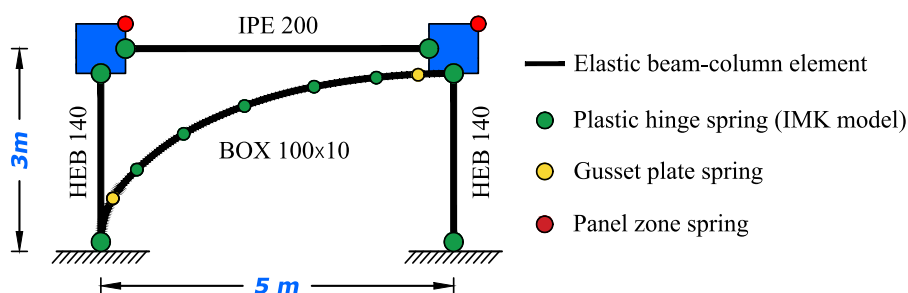

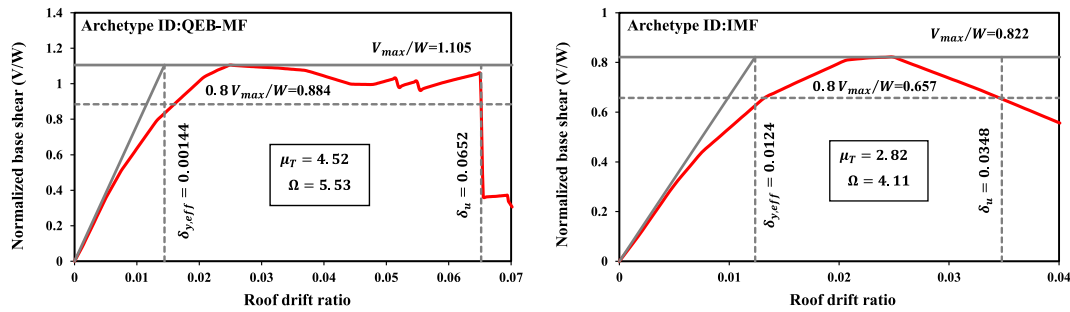**Fig. 14.** QEB-MF system modeling approach in OpenSees.

Fig. 15. Pushover curves of archetypes.

each of which with two translational degrees of freedom and one rotational degree of freedom. In addition, multi-point constraints (MPCs) were for pinned connections of the quarter-elliptic brace. And, S235JR steel was used for all parts, the specifications of which are provided in Table 3 according to EN1993-1–1 standard [39].

First, the lateral displacement of the studied frame in both software was obtained in accordance with Fig. 13. Then, using the stiffness equation and assuming the lateral force as 10,000 N, the elastic stiffness of these frames was calculated in Eq. (104) and Eq. (105). In Abaqus software and according to Fig. 13a, the lateral stiffness of QEB-MF system is obtained as follows:

$$K = \frac{P}{\Delta} = \frac{10000}{1.4137} = 7073.63 \frac{N}{mm} \tag{104}$$

In SAP2000 software and according to Fig. 13b, the lateral stiffness of QEB-MF system is obtained as follows:

$$K = \frac{P}{\Delta} = \frac{10000}{1.4124} = 7080.14 \frac{N}{mm} \tag{105}$$

Also, the lateral stiffness of QEB-MF system was calculated using the proposed relation in this study in Table 4:

Comparing the results of the analysis of the two finite element software and the proposed relation in this study for QEB-MF system shows that the error percentage is less than 1.5 %. This error is due to considering the shear shape coefficient of the cross-sections (α) and simplifications in equations. If the shear shape coefficient of the cross-sections equals zero, the difference between results will be negligible.

5. Seismic performance evaluation of the QEB-MF system

In this section, to evaluate the seismic performance of the steel moment frames equipped with quarter-elliptic braces, a single-span and single-story frame from a three-dimensional archetype designed in the seismic design category (SDC) D$_{max}$ with a response modification factor of 5 has been selected. Gravitational dead and live loads for the design of this archetype are considered 500 kgf/m^2 and 200 kgf/m^2, respectively, and S235JR steel is used for all cross-sections. Non-linear modeling has been done in OpenSees software, which meets the requirements of FEMA P695 methodology for modeling and analysis [40]. Concentrated plastic hinge modeling is used to show the softening and deterioration of the studied frames; based on this method, plastic hinges are placed at both ends of the columns and beams, and the middle element is modeled elastically. Quarter-elliptic member with twelve elements and five plastic hinges is modeled, so a plastic hinge is placed at one end of each element. The eight-element Krawinkler model was used to model the panel zone in the moment frame system [41]. The axial load ratio, which is defined as applied axial load (N) to axial load capacity (N_y) at a compressive cross-section, according to Jouneghani et al.'s studies on elliptical braces has been considered equal to 0.4 and 0.3 in Lignos relations for columns and bracing member, respectively [42]. A tiny percentage of rigidity has been considered in the bracing members' connections to gusset plates because these connections are not fully

jointed. According to Fig. 14, HEB 140, IPE 200, and BOX 100 × 100 × 10 cross-sections were used for columns, beam, and quarter-elliptic bracing member, respectively. In all members, the moment-rotation behavior of the concentric hinges is considered based on the modified Ibarra-Medina-Krawinkler (IMK) deterioration model with a bilinear hysteretic response [43–45].

In the following, to evaluate the seismic performance of the QEB-MF system, non-linear static analysis (pushover) and incremental dynamic analysis (IDA) are performed on the QEB-MF and IMF systems, and the results are compared.

5.1. Non-linear static analysis (pushover)

Nonlinear static analysis is performed under lateral static loads and gravity loads. First, gravity loads are placed on the structure, and then the structure is subjected to the lateral loading pattern. In the non-linear static analysis, according to FEMA P695, gravity load is applied on the structure using the load combination in Eq. (106):

$$1.05D + 0.25L \tag{106}$$

In this equation, D is the nominal dead load, and L is the nominal live load. The above equation coefficients represent the expected values of loads with normal probability distribution. Then, in this analysis, the distribution of the lateral force equivalent to the earthquake at the structure's height corresponding to the structure's first mode and the effective mass of the floors is performed according to Eq. (107):

$$F_x \propto m_x \varphi_{1,x} \tag{107}$$

where F_x is the lateral force distribution in height at each floor level (x), m_x is the structure's mass at level x, and $\varphi_{1,x}$ is the first mode of the structure at level x. The pushover curve of the QEB-MF and IMF systems is shown in Fig. 15. In this figure, V_{max}/w is equal to the maximum amount of base shear normalized by weight, δ_u is equal to the roof displacement at the point where 20 % of the maximum base shear is reduced, and $\delta_{y,eff}$ is the effective yield displacement of the roof calculated according to FEMA P695 methodology [40].

The over-strength factor, Ω, according to Eq. (108), is equal to the ratio of the maximum base shear (V_{max}) to the design base shear (V):

$$\Omega = \frac{V_{max}}{V} \tag{108}$$

Also, period-based ductility, μ_T, based on Eq. (109) is equal to the ratio of the ultimate displacement of the roof (δ_u) to the effective yield displacement of the roof ($\delta_{y,eff}$):

$$\mu_T = \frac{\delta_u}{\delta_{y,eff}} \tag{109}$$

The comparison of two push-over curves in Fig. 15 shows that adding a quarter-elliptic brace to the moment frame system has improved performance, increased elastic stiffness, increased maximum base shear, and increased ultimate displacement of this structural system.
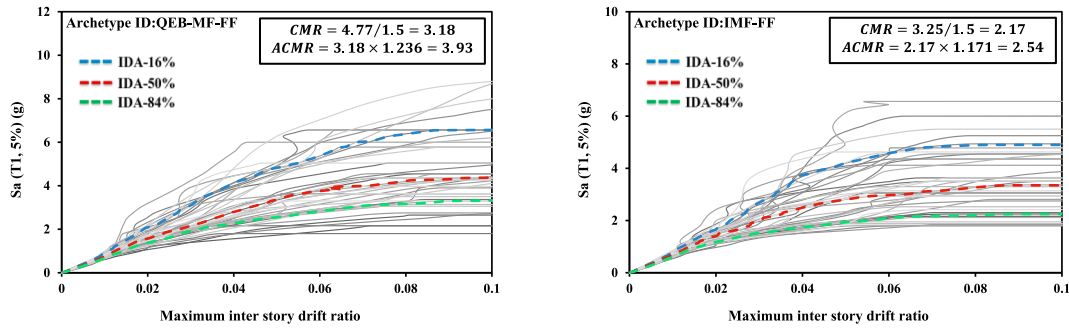
Fig. 16. IDA curves for QEB-MF and IMF archetypes under far-field ground motion records.
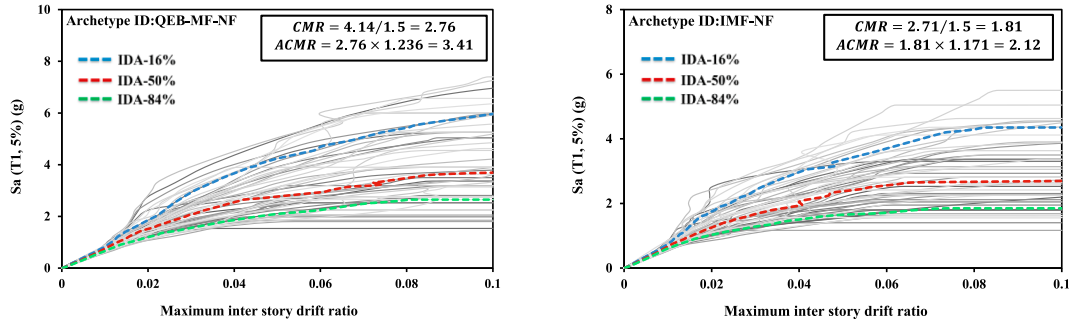

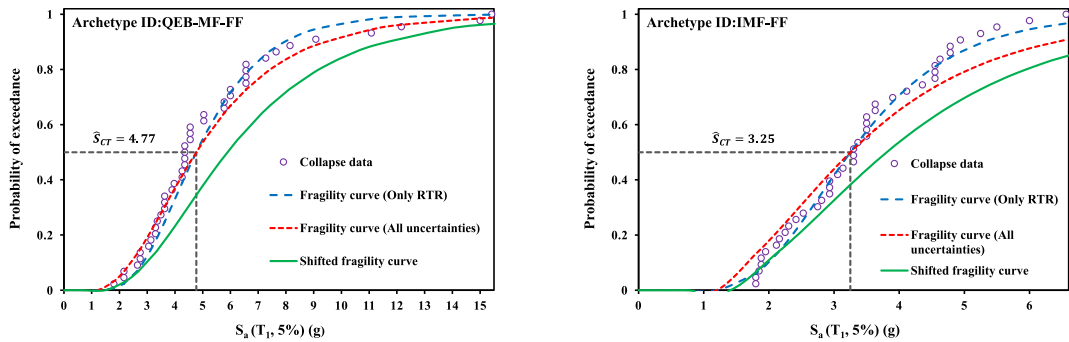**Fig. 17.** IDA curves for QEB-MF and IMF archetypes under near-field ground motion records.

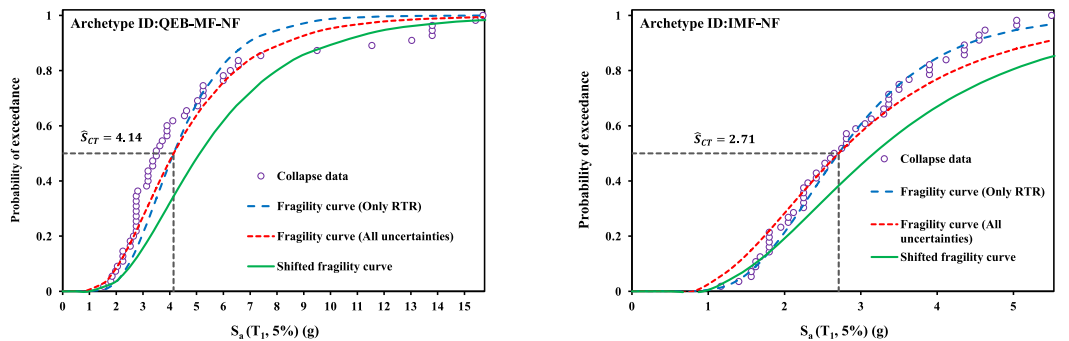**Fig. 18.** Fragility curves for QEB-MF and IMF archetypes under far-field ground motion records.

Fig. 19. Fragility curves for QEB-MF and IMF archetypes under near-field ground motion records.

5.2. Incremental dynamic analysis (far field and near field ground motion records)

In the method presented in the FEMA P695 methodology to evaluate

the seismic performance of structures, the median collapse capacity and safety margin are determined using incremental dynamic analysis [40]. In this study, the selected parameters for damage measure (DM) and intensity measure (IM), respectively, are maximum inter-story drift ratio

(MIDR) and first mode-5 % damped spectral acceleration, $S_a(T_1, 5\%)$. The median collapse capacity of each structure, $\widehat{S}_{CT}$, is calculated using IDA analysis under specific records, and the collapse margin ratio (CMR) is obtained according to the following equation:

$$CMR = \frac{\widehat{S}_{CT}}{S_{MT}} \tag{110}$$

In this equation, S_{MT} is the maximum considered earthquake (MCE) ground motion intensity, which in this research is equal to 1.5 for models based on structural period (T_1) and SDC D_{max}, according to FEMA P695. In order to consider the effects of frequency content (spectral shape) and adjust the records used, the CMR index is multiplied by a parameter called the spectral shape factor (SSF) to obtain the adjusted collapse margin ratio (ACMR). SSF values are calculated using FEMA P695 tables based on T_1 and μ_T.

$$ACMR = CMR \times SSF \tag{111}$$

The criteria for acceptance of the collapse performance of structural systems depend on the total amount of uncertainties involved in the performance evaluation process. These uncertainties include record-to-record uncertainty (β_{RTR}), modeling uncertainty (β_{MDL}), test data uncertainty (β_{TD}), and design requirements uncertainty (β_{DR}). In this study, according to FEMA P695 methodology, β_{MDL}, β_{TD} and β_{DR} are considered equal to 0.2 for the good quality level. β_{RTR} is considered equal to 0.4 for structures with μ_T greater than 3, and for structures with μ_T smaller than 3, the following equation is used to calculate this uncertainty:

$$0.2 \leq \beta_{RTR} = 0.1 + 0.1\mu_T \leq 0.4 \tag{112}$$

Because the four mentioned uncertainty sources are independent of each other, their total standard deviation is geometrically added to obtain the total collapse uncertainty (β_{TOT}):

$$\beta_{TOT} = \sqrt{\beta_{RTR}^2 + \beta_{MDL}^2 + \beta_{TD}^2 + \beta_{DR}^2} \tag{113}$$

In order to compare the seismic performance of the moment frame system with quarter-elliptic brace and without brace under the influence of far-field and near-field ground motion records, from the set of records proposed by FEMA P 695, including 22 pairs of far-field records and 28 pairs of near-field records (with and without pulses) is used. Also, the advanced "hunt and fill" algorithm was used to perform an optimal and intelligent scale for the intensity measure. The initial step, step increment, and the allowed number of runs per record in the hunt and fill algorithm were considered equal to 0.05, 0.05, and 30, respectively [46]. Fig. 16 shows IDA curves with 16 %, 50 %, and 84 % fractile curves under 44 far-field records, and Fig. 17 shows IDA curves with 16 %, 50 %, and 84 % fractile curves under 56 near-field records.

The acceptable collapse margin ratio (ACMR$_{10\%}$) for QEB-MF and IMF archetypes according to FEMA P695 and uncertainties are obtained as 1.97 and 1.93, respectively. Therefore, the criterion ACMR > ACMR$_{10\%}$ is passed per archetype. Examining the IDA analysis results of the archetypes shows that the use of quarter-elliptic braces in the moment frame system increases $\widehat{S}_{CT}$ and, as a result, increases ACMR and improves the seismic performance of these systems. Using these braces increases the ACMR by 54.72 % for far-field ground motion records and 60.85 % for near-field ground motion records in the moment frame system.

5.3. Collapse fragility evaluation

The collapse probability of structures for different intensity measures is displayed using fragility curve. It shows the collapse probability for each spectral acceleration level. The fragility curve is plotted considering a cumulative distribution function (CDF) from IDA results. The lognormal collapse fragility is determined by two main factors: the median collapse intensity $(\widehat{S}_{CT})$ and the standard deviation of the natural

logarithm. Fig. 18 shows the fragility curve for archetypes under far-field ground motion records, and Fig. 19 shows the fragility curve for archetypes under near-field ground motion records.

In these figures, two dashed fragility curves are drawn by considering β_{RTR} and β_{TOT} (all uncertaintiesas) the standard deviation parameter in the lognormal cumulative distributive function. Also, the solid curve (shifted fragility curve) is drawn by multiplying the fragility curve with the standard deviation parameter β_{TOT} in SSF. The fragility curve slope has increased with the median collapse intensity $(\widehat{S}_{CT})$ increase and the standard deviation increase.

6. Conclusions

In this research, the new quarter-elliptic brace was introduced. The stiffness and stability of the steel moment frame equipped with quarter-elliptic brace have been investigated analytically and numerically with an innovative new method. To this end, a new and completely accurate analytical formulation is presented using the concept of strain energy and Castigliano's theorem in order to calculate the elastic lateral stiffness of a two-dimensional single-span and single-story quarter-elliptic-braced steel moment frame (QEB-MF) under lateral load and taking into account all effective factors, including axial and shear forces as well as bending moment, for all the frame members. Then, the accuracy of this relation was investigated and controlled by means of modeling of QEB-MF system by OpenSees software and assigning 40 different values for the ratio of moment of inertia of strong axis of beam to moment of inertia of strong axis of column and 40 different values for the ratio of modification coefficients of quarter-elliptic bracing member to beams by MATLAB programming code. And also, using two finite element software, a numerical example was solved, and the obtained results were compared with the results obtained from the proposed relation. The error percentage is less than 1.5 % which shows that the accuracy and reliability of the proposed relation are high; therefore, by having the geometric specifications of column, beams, and quarter-elliptic bracing member cross-sections and having material properties, the elastic stiffness of the QEB-MF system under the lateral load can be easily calculated with conservative considerations considering the uncertainties. Then, the seismic performance of this system was investigated according to the FEMA P695 methodology for near-field and far-field ground motion records compared with the intermediate moment frame (IMF). For this purpose, first, non-linear static analysis was performed on the archetypes, and over-strength factor and period-based ductility were calculated using pushover curves. Next, IDA analysis was performed for 44 far-field and 56 near-field ground motion records, and fragility curves were drawn using the collapse data. The comparison of the obtained results showed that adding a quarter-elliptic brace to the moment frame system increases ACMR (54.72 % for far-field ground motion records and 60.85 % for near-field ground motion records) and thus improves the seismic performance of this system.

Declaration of Competing Interest

The authors declare that they have no known competing financial interests or personal relationships that could have appeared to influence the work reported in this paper.

References

[1] Sen AD, Roeder CW, Lehman DE, Berman JW. Nonlinear modeling of concentrically braced frames. J Constr Steel Res 2019;157:103–20. https://doi.org/10.1016/j.jcsr.2019.02.007.

[2] Kazemzadeh Azad S, Topkaya C, Astaneh-Asl A. Seismic behavior of concentrically braced frames designed to AISC341 and EC8 provisions. J Constr Steel Res 2017; 133:383–404. https://doi.org/10.1016/j.jcsr.2017.02.026.

[3] Ebadi P, Sabouri-Ghomi S. Conceptual study of X-braced frames with different steel grades using cyclic half-scale tests. J Earthq Eng Eng Vib 2012;11:313–29. https://doi.org/10.1007/sl1803-012-0124-2.

[4] Mahmoudi M, Mehrizi AZ, Shirpour A. Evaluation of the Effect of End-Connection Specifications on Lateral Bearing Capacity of Concentrically Braced Steel Frames. Int J Steel Struct 2018;18:179–87. https://doi.org/10.1007/s13296-018-0314-5.

[5] Kumar MS, Senthilkumar R, Sourabha L. Seismic performance of special concentric steel braced frames. Structures 2019;20:166–75. https://doi.org/10.1016/j.istruc.2019.03.012.

[6] Faytarouni M, Shen J, Seker O, Akbas B. Improved brace fracture model for seismic evaluation of concentrically braced frames. Eng Struct 2020;206:110184. https://doi.org/10.1016/j.engstruct.2020.110184.

[7] Fanaie N, Sadegh Kolbadi M, Afsar Dizaj E. Probabilistic Seismic Demand Assessment of Steel Moment Resisting Frames Isolated by LRB. *Numer Methods Civ Eng* 2017;2:52–62. doi:10.29252/nmce.2.2.52.

[8] Bastami M, Ahmady JR. Development of centrically fused braced frame (CFBF) for seismic regions. Soil Dyn Earthq Eng 2019;127:105856. https://doi.org/10.1016/j.soildyn.2019.105856.

[9] Fanaie N, Dizaj EA. Response modification factor of the frames braced with reduced yielding segment BRB. Struct Eng Mech 2014;50:1–17. https://doi.org/10.12989/sem.2014.50.1.001.

[10] Afsar Dizaj E, Fanaie N, Zarifpour A. Probabilistic seismic demand assessment of steel frames braced with reduced yielding segment buckling restrained braces. Adv Struct Eng 2018;21:1002–20. https://doi.org/10.1177/1369433217737115.

[11] Kachooee A, Kafi MA. A Suggested Method for Improving Post Buckling Behavior of Concentric Braces Based on Experimental and Numerical Studies. Structures 2018;14:333–47. https://doi.org/10.1016/j.istruc.2018.04.003.

[12] Mahmoudi M, Shirpour A, Zarezadeh A. The Effects of Mid-Span Connection Specifications on Compressive Performance of Cross (X) Braces. Int J Steel Struct 2019;19:1125–33. https://doi.org/10.1007/s13296-018-0192-x.

[13] Qiu C, Du X. Seismic performance of multistory CBFs with novel recentering energy dissipative braces. J Constr Steel Res 2020;168:105864. https://doi.org/10.1016/j.jcsr.2019.105864.

[14] Legeron F, Desjardins E, Ahmed E. Fuse performance on bracing of concentrically steel braced frames under cyclic loading. J Constr Steel Res 2014;95:242–55. https://doi.org/10.1016/j.jcsr.2013.12.010.

[15] Payandehjoo B, Ghasemzadeh H. Numerical Methods in Civil Engineering Analytical approach of buckling strength of yielding damped braced 2017;1.

[16] Moghaddam HA, Estekanchi HE. On the characteristics of an off-centre bracing system. J Constr Steel Res 1995;35:361–76.

[17] Moghaddam HA, Estekanchi HE. Seismic behaviour of offcentre bracing systems. J Constr Steel Res 1999;51:177–96. https://doi.org/10.1016/S0143-974X(99)00007-3.

[18] Trombetti T, Silvestri S, Gasparini G, Ricci I. Stiffness-Strength-Ductility-Design Approaches for Crescent Shaped Braces. Open Constr Build Technol J 2009;3:127–40. https://doi.org/10.2174/1874836800903020127.

[19] Fintel M, Khan FR. Shock-absorbing soft story concept for multistory earthquake structures. J Proc 1969;66:381–90.

[20] Palermo M, Silvestri S, Gasparini G, Trombetti T. Crescent shaped braces for the seismic design of building structures. Mater Struct Constr 2015;48:1485–502. https://doi.org/10.1617/s11527-014-0249-z.

[21] Palermo M, Pieraccini L, Dib A, Silvestri S, Trombetti T. Experimental tests on Crescent Shaped Braces hysteretic devices. Eng Struct 2017;144:185–200. https://doi.org/10.1016/j.engstruct.2017.04.034.

[22] Jouneghani HG, Haghollahi A, Moghaddam H, Moghadam AS. Study of the seismic performance of steel frames in the elliptic bracing. J Vibroeng 2016;18:2974–85. https://doi.org/10.21595/jve.2016.16858.

[23] Jouneghani HG, Haghollahi A. Assessing the seismic behavior of steel moment frames equipped by elliptical brace through incremental dynamic analysis (IDA). Earthq Eng Eng Vib 2020;19:435–49. https://doi.org/10.1007/s11803-020-0572-z.

[24] Jouneghani HG, Haghollahi A, Beheshti-Aval SB. Experimental study of failure mechanisms in elliptic-braced steel frame. Steel Compos Struct 2020;37:175–91.

[25] Boostani M, Rezaifar O, Gholaki M. Introduction and seismic performance investigation of the proposed lateral bracing system called "OGrid". Arch Civ Mech Eng 2018;18:1024–41. https://doi.org/10.1016/j.acme.2018.02.003.

[26] Boostani M, Rezaifar O, Gholaki M. Seismic performance investigation of new lateral bracing system called "OGrid-H". SN Appl Sci 2019;1:1–24. https://doi.org/10.1007/s42452-019-0369-8.

[27] Shamivand A, Akbari J. Ring-Shaped Lateral Bracing System for Steel Structures. Int J Steel Struct 2020;20:493–503. https://doi.org/10.1007/s13296-019-00299-z.

[28] Davis R, Henshell RD, Warburton GB. Curved beam finite elements for coupled bending and torsional vibration. Earthq Eng Struct Dyn 1972;1:165–75. https://doi.org/10.1002/eqe.4290010205.

[29] Davis R, Henshell RD, Warburton GB. Constant curvature beam finite elements for in-plane vibration. J Sound Vib 1972;25:561–76. https://doi.org/10.1016/0022-460X(72)90478-6.

[30] Yoo CH, Fehrenbach JP. Natural frequencies of curved girders. J Eng Mech Div 1981;107:339–54.

[31] Yang Y-B, Kuo S-R. Discussion: Thin-Walled Curved Beams. I: Formulation of Nonlinear Equations. J Eng Mech 1996;122:482–4. https://doi.org/10.1061/(asce)0733-9399(1996)122:5(482).

[32] Yoon KY, Park NH, Choi YJ, Kang YJ. Natural frequencies of thin-walled curved beams. Finite Elem Anal Des 2006;42:1176–86. https://doi.org/10.1016/j.finel.2006.05.002.

[33] Kim BY, Kim CB, Song SG, Beom HG, Cho C. A finite thin circular beam element for out-of-plane vibration analysis of curved beams. J Mech Sci Technol 2009;23:1396–405. https://doi.org/10.1007/s12206-008-1213-2.

[34] Rezaiee M, Rajabzadeh N. An Explicit Stiffness Matrix for Parabolic Beam Element. Lat Am J Solids Struct 2016;13:1782–801.

[35] Marotta E, Salvini P. Analytical Stiffness Matrix for Curved Metal Wires. Procedia Struct Integr 2018;8:43–55. https://doi.org/10.1016/j.prostr.2017.12.007.

[36] Hibbeler RC, Kiang T. Structural analysis. Pearson Prentice Hall Upper Saddle River; 2015.

[37] Mazzoni S, McKenna F, Scott MH, Fenves GL. OpenSees command language manual. Pacific Earthq Eng Res Cent 2006;264:137–58.

[38] Simulia DS. Abaqus 6.14 user's manual. Dassault Systems, Providence, RI; 2014.

[39] EN 1993-1-1. Eurocode 3: Design of steel structures - Part 1-1: General rules and rules for buildings. vol. 1. European Committee for Standardisation, Brussels; 2005.

[40] FEMA P695. Quantification of building seismic performance factors 2009.

[41] NIST 2017b. Guidelines for Nonlinear Structural Analysis for Design of Buildings Part IIa–Steel Moment Frames 2017.

[42] Ghasemi Jouneghani H, Haghollahi A, Moghaddam H, Sarveghad Moghadam A. Assessing Seismic Performance of the Elliptic Braced Moment Resisting Frame through Pushover Method. J Rehabil Civ Eng 2019;7:68–85. https://doi.org/10.22075/JRCE.2018.13030.1232.

[43] Lignos DG, Krawinkler H. A steel database for component deterioration of tubular hollow square steel columns under varying axial load for collapse assessment of steel structures under earthquakes. Proc. 7th Int. Conf. Urban Earthq. Eng; 2010.

[44] Lignos DG, Krawinkler H. Deterioration modeling of steel components in support of collapse prediction of steel moment frames under earthquake loading. J Struct Eng 2011;137:1291.

[45] Lignos DG, Asce M, Hartloper AR, Asce SM, Elkady A, Asce AM, et al. Proposed Updates to the ASCE 41 Nonlinear Modeling Parameters for Wide-Flange Steel Columns in Support of Performance-Based Seismic. Engineering 2019;145:1–13. https://doi.org/10.1061/(ASCE)ST.1943-541X.0002353.

[46] Vamvatsikos D, Cornell CA. Incremental dynamic analysis. Earthq Eng Struct Dyn 2002;31:491–514.